The mutation frequency was high (21%) in T4 cancers and very low (6%) in T2 cancers. Mutations in exons 1, 9 and 20 were detected in 5 (2%), 9 (4%) and 7 (3%) cases, respectively. Two new types of PIK3CA mutation, R88Q and R108H, were found in exon1. All PIK3CA mutations were heterozygous missense single-base substitutions, the most common being H1047R (6/20, 30%) in exon20. Eighteen cancers (8%) were EBV-positive and this positivity significantly correlated with a diffuse histological type (13/18 *vs* 93/198, P = 0.04). There were 7 cases of lymphoepithelioma-like carcinomas (LELC) and 6 of those cases were EBV-positive (percent/EBV: 6/18, 33%; percent/all LELC: 6/7, 86%). pAkt expression was positive in 119 (53%) cases but showed no correlation with clinicopathological characteristics. pAkt expression was significantly correlated with HER2 overexpression (16/20 *vs* 103/211, P < 0.01) but not with PIK3CA mutations (12/20 *vs* 107/211, P = 0.37) or EBV infection (8/18 *vs* 103/211, P = 0.69). The frequency of pAkt expression was higher in cancers with exon20 mutations (100%) than in those with exon1 (40%) or exon9 (56%) mutations. One case showed both HER2 overexpression and EBV infection and 3 cases showed both PIK3CA mutations and EBV infection. However, no cases showed both PIK3CA mutations and HER2 overexpression. One EBV-positive cancer with PIK3CA mutation (H1047R) was MSI-positive. Three of these 4 cases were positive for pAkt expression. In survival analysis, pAkt expression significantly correlated with a poor prognosis (hazard ratio 1.75; 95%CI: 1.12-2.80, P = 0.02).

CONCLUSION: HER2 expression, PIK3CA mutations and EBV infection in gastric cancer were characterized. pAkt expression significantly correlates with HER2 expression and with a poor prognosis.

Key words: Human epidermal growth factor receptor 2; Phosphatidylinositol 3-kinase; Catalytic; Alpha polypeptide; Epstein-Barr virus; Akt; Gastric cancer

Peer reviewer: Takaaki Arigami, MD, PhD, Department of Surgical Oncology and Digestive Surgery, Field of Oncology, Kagoshima University Graduate School of Medical and Dental Sciences, 8-35-1 Sakuragaoka, Kagoshima 891-0175, Japan

Sukawa Y, Yamamoto H, Nosho K, Kunimoto H, Suzuki H, Adachi Y, Nakazawa M, Nobuoka T, Kawayama M, Mikami M, Matsuno T, Hasegawa T, Hirata K, Imai K, Shinomura Y. Alterations in the human epidermal growth factor receptor 2-phosphatidylinositol 3-kinase-v-Akt pathway in gastric cancer. *World J Gastroenterol* 2012; 18(45): 6577-6586 Available from: URL: http://www.wjgnet.com/1007-9327/full/v18/i45/6577.htm DOI: http://dx.doi.org/10.3748/wjg.v18.i45.6577

INTRODUCTION

Gastric cancer is one of the most common cancer types and the second leading cause of cancer-related deaths worldwide[1]. Genetic and epigenetic alterations play important roles in the development and progression of these tumors[1,2]. Considerable attention has been given to the potential role of the phosphatidylinositol 3-kinase (PI3K)-Akt signaling pathway in gastric cancer[3,4]. Various alterations, such as activation of growth factor receptors, PI3K, catalytic, alpha polypeptide (PIK3CA) mutations and inactivation of phosphatase and tensin homolog (PTEN) lead to activation of the PI3K-Akt signaling pathway. With regards to growth factor receptors, there is growing evidence that human epidermal growth factor receptor 2 (HER2) is a key driver of tumorigenesis and an important biomarker in gastric cancer. The amplification or overexpression of HER2 is observed in 7%-34% of these cases[5-9].

PIK3CA is mutated in a wide variety of human tumor types[10,11], including gastric cancers[12-15]. Activating mutations in this gene up-regulate the PI3K-Akt signaling pathway, making it a potentially useful therapeutic target. For example, oncogenic mutations of PIK3CA reportedly render breast cancers more resistant to treatment with the anti-HER2 receptor antibody trastuzumab[16]. Thus, this signaling pathway is thought to be one of the mechanisms underlying resistance to trastuzumab. Trastuzumab has recently been approved for treatment of advanced gastric cancers[5,6].

Pyrosequencing-based methods facilitate the identification of low-frequency tumor mutations and allow a more accurate assessment of tumor mutation burden[17]. PIK3CA mutations have been detected in 4%-25% of gastric cancers[12-15]. However, in most previous studies, only exons 9 and 20 hot spot mutations in PIK3CA were analyzed by DNA sequencing. Moreover, the association between HER2 expression and PIK3CA mutations in gastric cancer has not been reported.

A significant correlation has been found between Epstein-Barr virus (EBV) and the methylation of multiple genes in gastric cancers[18-20]. EBV infection reportedly induces PTEN expression loss through CpG island methylation of its promoter, leading to activation of the PI3K-Akt signaling pathway, in EBV-associated gastric cancer[21].

The aim of our present study was to systematically characterize HER2 expression, PIK3CA mutations, and EBV infection, all of which are involved in the PI3K-Akt signaling pathway, in a large cohort of gastric cancers (n = 231). We wished to determine the prevalence of each of these factors with a high precision and thereby correlate them with clinicopathological and molecular features of gastric lesions, including microsatellite instability (MSI) and phospho Akt (pAkt) expression.

MATERIALS AND METHODS

Tissue samples

A total of 231 formalin-fixed, paraffin-embedded (FFPE) gastric cancer tissue specimens from Japanese patients who had undergone surgical treatment was analyzed in

Table 1 Clinicopathological characteristics of patients with gastric cancer

Variables (n = 231)		n (%)
Sex	Male	157 (68)
	Female	74 (32)
Age (yr)	Median (range)	71 (25-91)
Location	Cardias	82 (35)
	Body	62 (27)
	Antrum	83 (36)
	Unknown	4 (2)
Depth of invasion	T2	125 (54)
	T3	92 (40)
	T4	14 (6)
Lymph node metastasis	N0	65 (28)
	N+	158 (68)
	N1	73 (32)
	N2	56 (24)
	N3	29 (13)
	Unknown	8 (3)
Stage	I B	49 (21)
	II	45 (19)
	IIIA + IIIB	82 (35)
	IV	51 (22)
	Unknown	4 (2)
Lauren histotype	Intestinal	113 (49)
	Diffuse	112 (48)
	Others	6 (3)

this study. The patients' age, sex, tumor location, depth of invasion, pathological type, lymph node metastasis, and pathological stage were determined by a review of their medical records. Clinicopathological findings were determined according to the criteria of the Japanese Research Society for Gastric Cancer (Table 1). Our institutional review committee approved the study.

Immunohistochemistry

HER2 expression was analyzed using the HercepTest™ kit (DAKO, Carpinteria, CA) by manual sample processing in accordance with the manufacturer's instructions. Standard criteria for HER2 positivity (0, 1+, 2+ and 3+) were used. Tumors that scored 3+ were considered HER2-positive. For the immunohistochemical analysis of pAkt, FFPE specimens were processed using SignalStain Boost Detection Reagent (Cell Signaling Technology, Beverly, MA). Briefly, 5-μm-thick sections were dewaxed in xylene, rehydrated in ethanol, and heated with target retrieval solution (DAKO) in an autoclave for antigen retrieval. Endogenous peroxidase was blocked by incubation with 0.3% hydrogen peroxide in methanol for 10 min. The tissue sections were then washed twice with tris-buffered saline (TBS) and preblocked with 10% goat serum in TBS for 60 min. After washing with TBS, the sections were incubated with an anti-phospho-Akt (Ser473) polyclonal antibody (D9E, Cell Signaling Technology) at a dilution of 1:100 for 30 h at 4 ℃. The sections were washed three times in TBS and incubated with SignalStain Boost Detection Reagent for 45 min. After three further washes in TBS, a diamino-benzidine tetrahydrochloride working solution was applied. Finally, the sections were counterstained with hematoxylin. Tumors were considered pAkt-positive when the percentage of positive tumor cells was 10% or more[22]. Only clear staining of the tumor cell nucleus and/or cytoplasm was considered positive.

Mutation analysis of the PIK3CA gene by pyrosequencing

Genomic DNA was extracted from tumor specimens and mutations in exon9 and exon20 of the *PIK3CA* gene were analyzed by pyrosequencing as described previously[23,24]. We also developed a pyrosequencing assay to detect PIK-3CA exon1 mutations using the primer sets exon1-RS1 (5'-GGGAAGAATTTTTTGATGAAACA-3' for the biotinylated forward primer and 5'-GGTTGCCTACT-GGTTCAATTACTT-3' for the reverse primer) and exon1-RS2 (5'-CGGCTTTTTCAACCCTTTTT-3' for the forward primer and 5'-ATTTCTCGATTGAG-GATCTTTTCT-3' for the biotinylated reverse primer). Each polymerase chain reaction (PCR) mix contained the forward and reverse primers (each 10 μmol/L), a 25 mmol/L dNTP mix with dUTP, 75 mmol/L $MgCl_2$, 1 × PCR buffer, 1.0 U of exTaq, and 2 μL of template DNA in a total volume of 25 μL. PCR conditions were as follows: initial denaturing at 95 ℃ for 5 min; 50 cycles of 94 ℃ for 20 s, 50 ℃ for 20 s and 74 ℃ for 40 s; and a final extension at 72 ℃ for 1 min. The PCR products (each 25 μL) were sequenced using the PyroMark kit and Pyrosequencing PSQ96 HS System (Qiagen, Valencia, CA).

In situ hybridization for EBER1

The presence of EBV in the carcinoma tissues was evaluated by *in situ* hybridization (ISH) targeting of EBV-encoded small RNA (EBER-ISH) with an EBER-RNA probe (Dako Cytomation).

Microsatellite instability analysis

MSI was analyzed by PCR using the mononucleotide markers (BAT25 and BAT26). Based on the number of markers showing instability per tumor sample, cancers were divided into two groups; those with one or more of the two markers displaying MSI and those with no instability (microsatellite stable).

Statistical analysis

For all statistical analysis, the JMP program was used. All P values were two-sided and statistical significance was set at $P \leq 0.05$. For categorical data, the χ^2 test was used. For survival analysis, Kaplan-Meier method and log-rank test were used. For analysis of cancer-specific mortality, we excluded surgery-related deaths (deaths within one month of surgery).

RESULTS

HER2 expression in gastric cancer tissues

HER2 expression levels of 0, 1+, 2+ and 3+ were found in 167 (72%), 32 (14%), 12 (5%) and 20 (8.7%) samples, respectively (Figure 1). HER2 overexpression (IHC 3+) significantly correlated with intestinal histological type

Table 2 Clinicopathological characteristics of patients with gastric cancer based on human epidermal growth factor receptor 2 expression, phosphatidylinositol 3-kinase, catalytic, alpha polypeptide mutations and Epstein-Barr virus infection *n* (%)

		HER2			PIK3CA			EBV		
		Positive (*n* = 20)	Negative (*n* = 211)	*P* value	Mutation (*n* = 20)	Wild type (*n* = 211)	*P* value	Positive (*n* = 18)	Negative (*n* = 204)	*P* value
Sex	Male	15 (75)	142 (67)	0.48	13 (65)	144 (68)	0.77	14 (78)	138 (68)	0.38
	Female	5 (25)	69 (33)		7 (35)	70 (32)		4 (22)	66 (32)	
Age	Median	69 (50-84)	71 (25-91)	0.26	71 (25-85)	70 (38-91)	0.40	72 (48-90)	70 (38-91)	0.41
Location	Cardias	10 (50)	72 (34)	0.49	5 (25)	77 (36)	0.31	8 (44)	73 (36)	0.70
	Body	5 (25)	57 (27)		4 (20)	58 (27)		5 (28)	55 (27)	
	Antrum	5 (25)	78 (37)		10 (50)	73 (35)		5 (28)	75 (37)	
	Unknown	0	4 (2)		1 (5)	2 (1)		0	1 (0)	
Depth	T2	12 (60)	113 (54)	0.48	8 (40)	117 (55)	0.15	12 (67)	106 (52)	0.35
	T3	8 (40)	84 (40)		9 (45)	83 (39)		6 (33)	85 (42)	
	T4	0	14 (6)		3 (15)	11 (5)		0	13 (6)	
L/N meta	N0	5 (25)	60 (28)	0.71	4 (20)	61 (29)	0.37	3 (17)	57 (28)	0.28
	N+	14 (70)	144 (68)		16 (80)	142 (67)		14 (77)	140 (69)	
	N1	5 (25)	68 (32)		8 (40)	65 (31)		8 (44)	63 (31)	
	N2	6 (30)	50 (24)		6 (30)	50 (24)		2 (11)	53 (26)	
	N3	3 (15)	26 (12)		2 (10)	27 (13)		4 (22)	24 (12)	
	Unknown	1 (5)	7 (3)		0	8 (4)		1 (6)	7 (3)	
Stage	I	5 (25)	44 (21)	0.89	1 (5)	48 (23)	0.14	3 (17)	41 (20)	0.98
	II	3 (15)	42 (20)		7 (35)	38 (18)		4 (22)	39 (19)	
	III	6 (30)	76 (36)		8 (40)	74 (35)		6 (33)	75 (37)	
	IV	5 (25)	46 (22)		4 (20)	47 (22)		4 (22)	46 (23)	
	Unknown	1 (5)	3 (1)		0	4 (2)		1 (6)	3 (1)	
Lauren	Intestinal	15 (75)	98 (46)	0.05	14 (70)	99 (47)	0.13	5 (28)	105 (51)	0.04
histotype	Diffuse	5 (25)	107 (51)		6 (30)	106 (50)		13 (72)	93 (46)	
	LELC	0	6 (3)		2 (10)	4 (2)		5 (28)	0	
	Others	0	6 (3)		0	6 (3)		0	6 (3)	
MSI		2 (10)	28 (13)	0.72	10 (50)	20 (9)	< 0.01	1 (6)	26 (13)	0.36
pAkt		16 (84)	103 (51)	< 0.01	12 (63)	107 (53)	0.37	8 (47)	103 (52)	0.69
3 yr OS (%)		29.4	59.2	0.24	57.3	56.8	0.59	57.4	57.3	0.98

MSI: Microsatellite instability; LELC: Lymphoepithelioma-like carcinoma; HER2: Human epidermal growth factor receptor 2; PIK3CA: Phosphatidylinositol 3-kinase, catalytic, alpha polypeptide mutations; EBV: Epstein-Barr virus; pAkt: Phospho Akt; OS: Overall survival.

Table 3 Frequencies of phosphatidylinositol 3-kinase, catalytic, alpha polypeptide mutations detected in gastric cancer tissues

	Mutation	Overall frequency	Percent/ total cases	Percent/ mutated cases	Microsatellite instability
Exon1	R88Q	1	0.4	5	1
	R108H	4	1.7	20	1
	Total	5	2.2		2
Exon9	E542K	5	2.2	25	1
	E545K	2	0.9	10	1
	E545G	2	0.9	10	1
	Total	9	4.0		3
Exon20	H1047Y	1	0.4	5	1
	H1047R	6	2.6	30	4
	Total	7	3.0		5

(15/20 *vs* 98/205, $P = 0.05$, Table 2). Three-year survival rates were 29% in patients with HER2 overexpression and 59% in cases without HER2 overexpression, respectively [hazard ratio (HR) 1.73; 95%CI: 0.87-3.14, $P = 0.24$].

Mutations of the PIK3CA gene in gastric cancer tissues

PIK3CA mutations were present in 20 cases (8.7%) (Table 2 and Figure 2). The mutation frequency was high (21%) in T4 cancers and low (6%) in T2 cancers. Mutations in exons 1, 9 and 20 of PIK3CA were detected in 5 (2%), 9 (4%) and 7 (3%) cases, respectively (Table 3). One case had multiple PIK3CA mutations (R108H and E542K). The exon20/exon9 prevalence ratio was 0.78 (7/9). Two new types of PIK3CA mutations, R88Q and R108H, were detected in exon1. All mutations were heterozygous missense single-base substitutions and the most common mutation was H1047R (6/20; 30%) in exon20. PIK3CA mutations were also found to significantly correlate with MSI (10/20 *vs* 9/211, $P < 0.01$) but not with other clinicopathological characteristics. The three-year survival rates were 57% in patients with PIK3CA mutations and 57% in cases without PIK3CA mutations, respectively (HR 1.37; 95%CI: 0.68-3.26, $P = 0.59$).

EBV infection

Eighteen samples in our cohort (8%) were EBV-positive and this positivity significantly correlated with diffuse histological type (13/18 *vs* 93/198, $P = 0.04$) (Table 2 and Figure 3). There were 7 cases of LELC and 6 of those cases were EBV-positive (percent/EBV: 6/18, 33%; percent/all LELC: 6/7, 86%). The three-year survival rates were 57% in patients with EBV infection and 57% in those without EBV infection (HR 0.81; 95%CI:

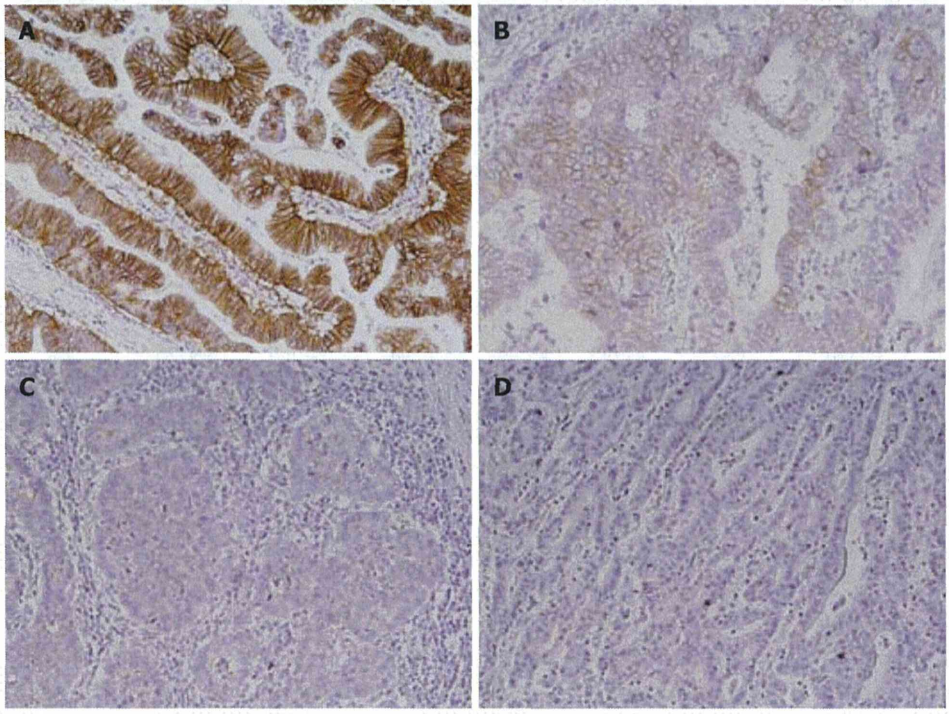

Figure 1 Immunohistochemical analysis of human epidermal growth factor receptor 2 in gastric cancer tissues. A: Human epidermal growth factor receptor 2 (HER2) 3+; B: HER2 2+; C: HER2 1+; D: HER2 0. Original magnification, ×200.

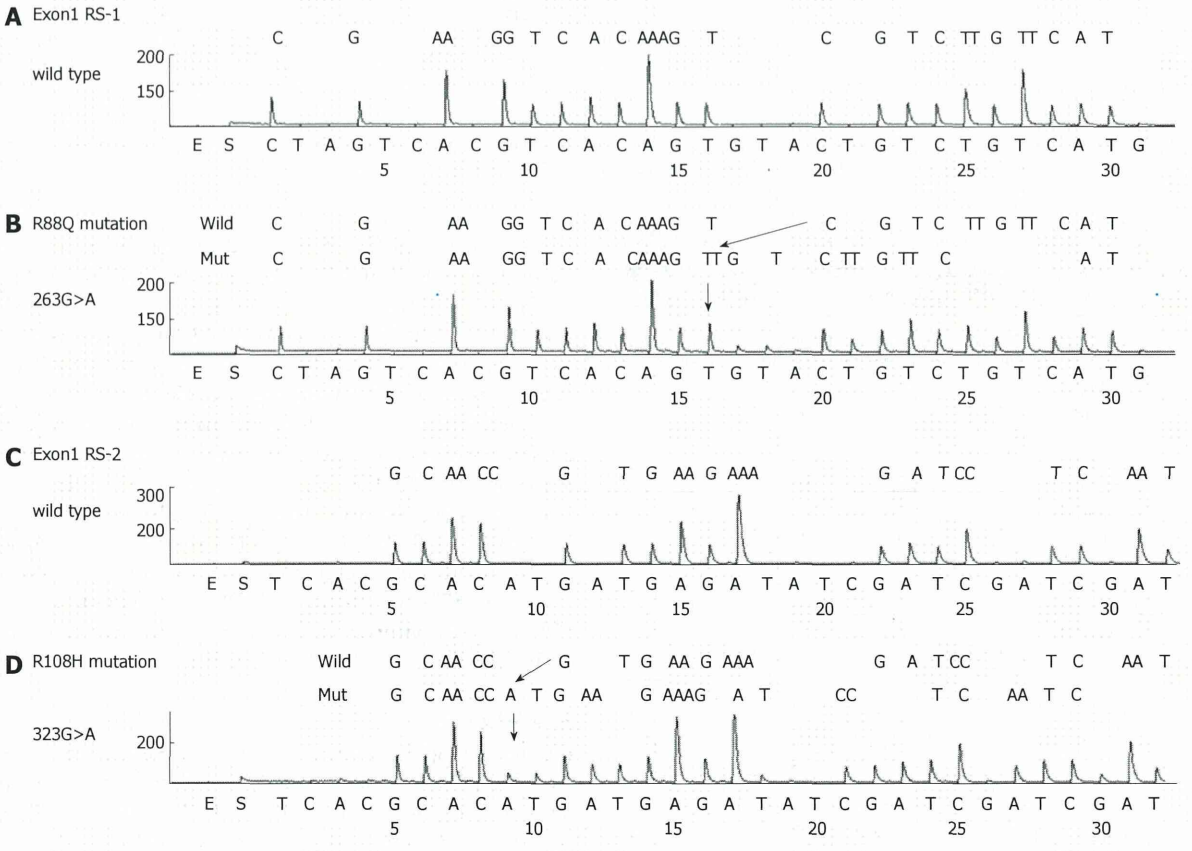

Figure 2 Phosphatidylinositol 3-kinase, catalytic, alpha polypeptide mutations detected by pyrosequencing in gastric cancer tissues. A: Exon1 RS1 wild type; B: 263G>A (R88Q) mutation; C: Exon1 RS2 wild type; D: 323G>A (R108H) mutation.

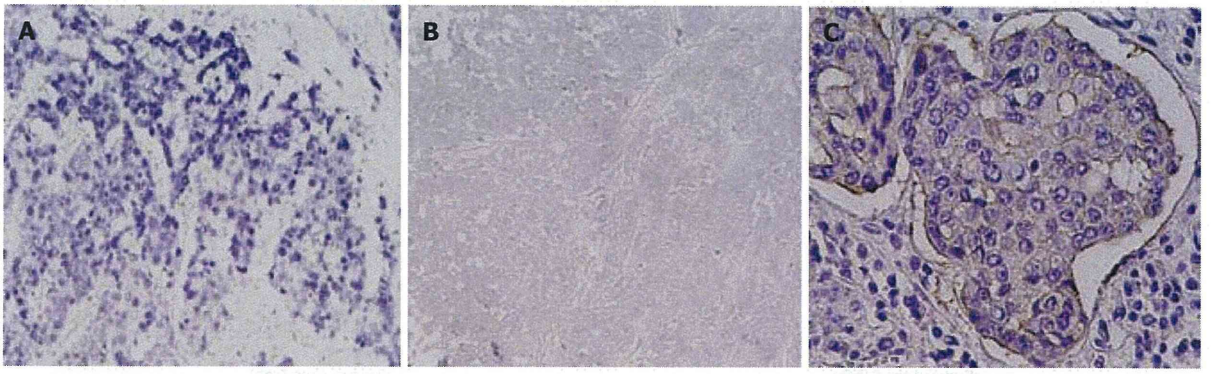

Figure 3 *In situ* hybridization analysis of Epstein-Barr virus-encoded small RNA-1 and human epidermal growth factor receptor 2 immunohistochemical expression in gastric cancer tissues. A: Gastric adenocarcinoma positive for Epstein-Barr virus-encoded small RNA-1 (EBER-1); B: Gastric adenocarcinoma negative for EBER-1; C: Immunohistochemical analysis of human epidermal growth factor receptor 2 (HER2) in an Epstein-Barr virus-positive and HER2-positive case. Original magnification, ×200.

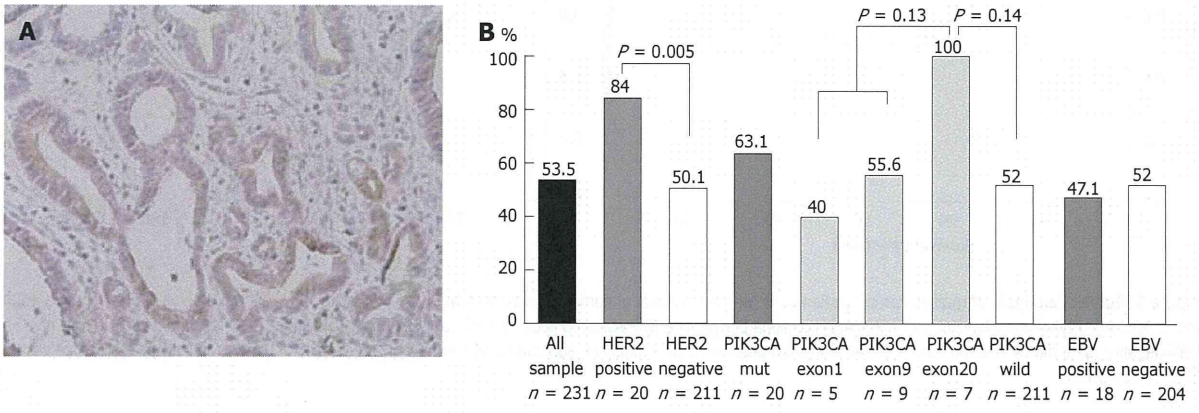

Figure 4 Immunohistochemical analysis and assessment of phospho Akt positivity based on molecular alterations in gastric cancer tissues. A: Gastric adenocarcinoma showing phospho Akt (pAkt) positivity. Original magnification, ×200; B: pAkt expression significantly correlates with human epidermal growth factor receptor 2 (HER2) overexpression ($P < 0.01$) but not with phosphatidylinositol 3-kinase, catalytic, alpha polypeptide (PIK3CA) mutations ($P = 0.37$) or Epstein-Barr virus (EBV) infection ($P = 0.69$).

0.36-2.31, $P = 0.98$).

Association of HER2 overexpression, PIK3CA mutations and EBV infection

One of our cases showed both HER2 overexpression and EBV infection and 3 cases showed both PIK3CA mutations and EBV infection. However there were no cases showing both PIK3CA mutations and HER2 overexpression. Three of the 4 cases were positive also for pAkt expression. PIK3CA mutations were present in 3 EBV-positive cancers, including 2 cases of LELC (2/5, 40%). One EBV-positive cancer with a PIK3CA mutation (H1047R) was MSI-positive.

pAkt expression

pAkt expression was positive in 119 (53%) of our cases but this showed no correlation with clinicopathological characteristics (Figure 4A). On the other hand, pAkt expression was found to be significantly correlated with HER2 overexpression (16/19 *vs* 103/204, $P < 0.01$) but not with PIK3CA mutations (12/19 *vs* 107/204, $P = 0.37$) or EBV infection (8/17 *vs* 103/198, $P = 0.69$) (Table 2). The frequency of pAkt expression was higher in cancers with exon20 mutations (100%) than in those with exon1 (40%) or exon9 (56%) mutations of PIK3CA, although this difference did not reach statistical significance (Figure 4B). The five-year survival rates were 37% in patients with pAkt expression and 59% in those without pAkt expression (HR 1.75; 95%CI: 1.12-2.80, $P = 0.02$) (Figure 5). Hence, pAkt expression significantly correlates with a poor prognosis in gastric cancer.

DISCUSSION

In our present study, we systematically characterized HER2 expression, PIK3CA mutations and EBV infection, all of which are involved in the PI3K-Akt signaling pathway, in a large cohort of patients with gastric cancer ($n = 231$). We aimed to determine the prevalence of these characteristics with a high level of precision and to correlate them with clinicopathological and molecular features, such as MSI and pAkt expression.

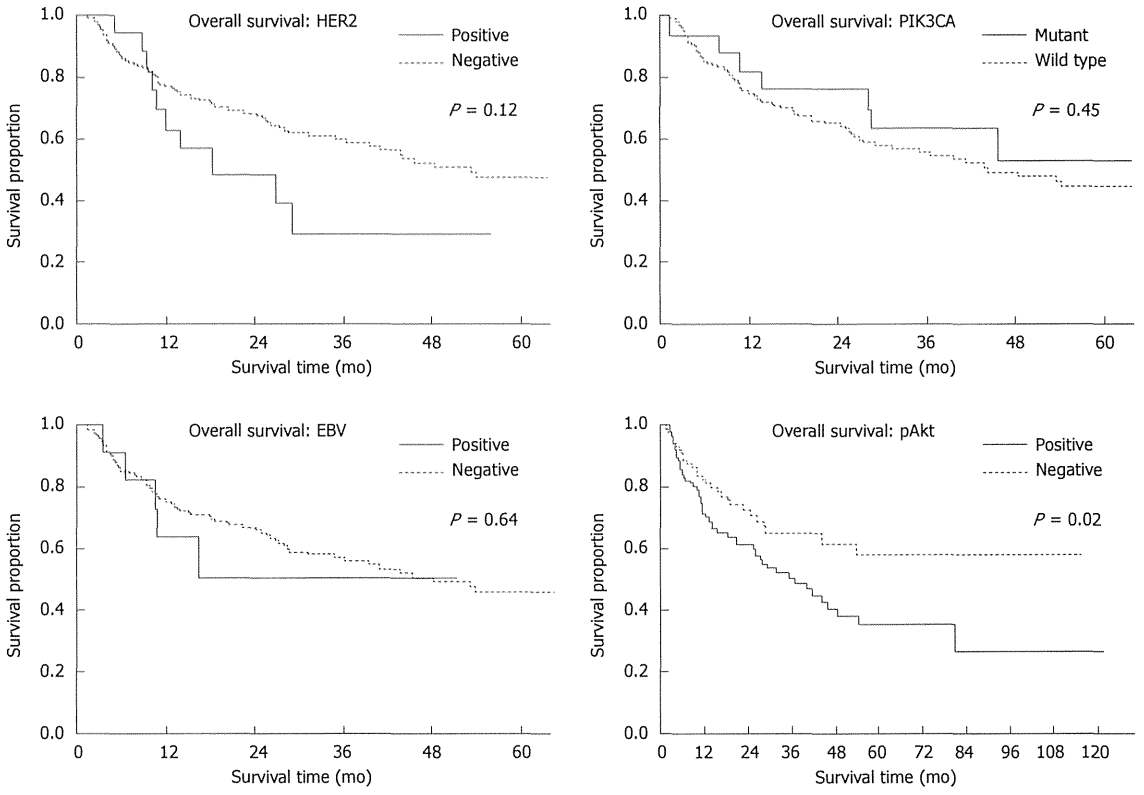

Figure 5 Survival analysis of gastric cancer patients. Three year survival of human epidermal growth factor receptor 2 (HER2)-positive *vs* HER2-negative, 29.1 mo *vs* 59.4 mo; Phosphatidylinositol 3-kinase, catalytic, alpha polypeptide (PIK3CA) mutation *vs* wild type, 63.7 mo *vs* 56.3 mo; Epstein-Barr virus (EBV)-positive *vs* EBV-negative, 51.3 mo *vs* 57.6 mo; And phospho Akt (pAkt)-positive *vs* pAkt-negative, 50.7 mo *vs* 64.8 mo. Five year survival of pAkt-positive *vs* pAkt-negative cases, 35.5 mo *vs* 58.1 mo.

HER2 overexpression (IHC 3+) was present in 20 samples (8.4%), a value that is within the range (7%-34%) reported in the current literature[5-9]. HER2 overexpression was found to significantly correlate with the intestinal histological type. Hence, the frequency of HER2 expression may depend on, at least in part, the distribution of histology in a cohort of gastric cancer samples. Some studies have suggested that HER2 positivity in gastric cancer is associated with poor outcomes and aggressive disease, but the results are conflicting. We found for the first time in our present analyses that HER2 overexpression significantly correlates with pAkt expression in gastric cancer tissues. Moreover, pAkt expression correlated with a poor prognosis in these patients. Thus, the HER2-Akt axis may play an important role in gastric cancer.

Pyrosequencing-based methods facilitate the identification of low-frequency tumor mutations and allow a more accurate assessment of tumor mutation burden[17,23,24]. We characterized PIK3CA mutations in gastric cancer tissues using pyrosequencing for the first time. The overall prevalence of PIK3CA mutations was found in our analysis to be 8.7%, a value that is within the previously reported range (4% to 25%)[10,12-15]. The mutation frequency was found to be high (21.4%) in T4 cancers and low (6.4%) in T2 cancers in our sample cohort. Thus, PIK3CA mutations appear to be late events in gastric carcinogenesis, leading to tumor progression. These patients might therefore be appropriate for targeted therapies directed against the PI3K pathway.

The most common PIK3CA mutation found in our analysis was H1047R, which was also found previously[15]. Importantly, two new types of mutations were found in exon1. To our knowledge, PIK3CA mutations involving residues 88 and 108 (R88Q and R108H) have been never reported previously in gastric cancer, nor described in the COSMIC database, despite the large number of previous studies in which this region was investigated. These mutations have been detected in several other types of cancer tissues[25]. Importantly also, these mutations have been reported to be gain-of-function[26-28]. Our present results thus have potential clinical implications since the mutational status of PIK3CA could stratify patients for genotype-based molecular therapies targeting the PI3K pathway. Hence, exon1 of PIK3CA should be analyzed in gastric cancer patients in these clinical settings.

PIK3CA mutations were found to be significantly associated with the MSI phenotype in our experiments. An association between PIK3CA mutations and MSI has been reported, or at least suggested, for both gastric and colon cancers[12,13,29]. We found in our present study that PIK3CA mutations in cancers with MSI are distributed in exon1, exon9 and exon20. These results further sup-

port the notion that PIK3CA is one of the most important oncogenes activated by missense mutations in MSI-positive gastric cancers.

The frequency of pAkt expression was found to be higher in cancers with exon20 mutations (100%) than in those with exon1 (40%) or exon9 (56%) mutations in PIK3CA. These results further support the notion that the functional significance of PIK3CA mutations depends on the mutation type and that the H1047R hotspot mutation has high oncogenic activity.

The previous ToGA study has shown that the addition of trastuzumab to the chemotherapeutic regimen improves survival in patients with advanced gastric or gastroesophageal junction cancer[5,6]. PIK3CA mutation is one of the mechanisms underlying the resistance to trastuzumab in breast cancer[30]. Trastuzumab is likely to be effective for HER2-overexpressing breast cancers with no PIK3CA mutations, with possible rescue using HER2-TKIs in cases of relapse[31]. For HER2-overexpressing breast cancer with PIK3CA mutations, inhibitors against molecules of the PI3K pathway are possibly more effective than anti-HER2 agents, which are unlikely to be beneficial[32]. In our present study, PIK3CA mutations were not found in gastric cancers with HER2 overexpression. Thus, it is unlikely that PIK3CA mutation is a major mechanism underlying the resistance to trastuzumab in gastric cancer.

HER2 overexpression was found in only one of the 18 EBV-positive gastric cancers in our sample cohort. This result can be explained, at least in part, by the fact that HER2 overexpression and EBV infection significantly correlate with intestinal and diffuse histological types, respectively. On the other hand, PIK3CA mutations were identified in 3 EBV-positive cancers, including 2 cases of LELC (2/5, 40%). Although not analyzed in our current study, EBV infection reportedly inactivates PTEN through the CpG island methylation of its promoter in EBV-associated gastric cancer[21]. Thus, alterations in the PI3K-Akt signaling pathway in EBV-positive gastric cancers may differ from those in EBV-negative cancers.

Finally, pAkt expression was found to correlate with a poor prognosis in gastric cancer. A significant association between increased pAkt expression and poor prognosis has been reported previously in patients with T3/T4 gastric cancer but not in those with T1/T2 cancer[33]. It has been reported also that pAkt expression is associated with increased resistance to multiple chemotherapeutic agents in gastric cancer patients, when chemotherapeutic sensitivities were tested using MTT assays[34]. Thus, Akt activation appears to lead to a poor prognosis and resistance to chemotherapeutic agents in gastric cancer. A positive correlation between a decrease in the pAkt levels after gefitinib administration and tumor apoptotic index in gastric cancer has also been reported[35]. Further analyses regarding the pAkt status in cancer tissues before and after chemotherapy and molecular targeted therapy will be necessary. Not all Akt activation events can be explained by HER2 expression, PIK3CA mutations, and EBV infection in gastric cancer. We have reported previously that a dominant negative insulin-like growth factor (IGF)-1 receptor blocks the Akt-1 activation induced by IGF-1 and IGF-2 in gastric cancer cell lines[36]. Thus, molecular alterations, such as the overexpression of IGF-1 receptor, might be involved in the activation of Akt in gastric cancer and this issue needs to be clarified in the near future.

COMMENTS

Background

Personalized therapy has begun also in advanced gastric cancer through the use of trastuzumab, an anti-human epidermal growth factor receptor 2 (HER2) antibody. Many drugs targeting the phosphatidylinositol 3-kinase (PI3K)-Akt pathway have now been developed and clinical trials are ongoing. An appropriate biomarker is necessary for successful molecular targeted therapy. The alterations of molecules in the PI3K-Akt pathway could be a good biomarker for such drugs.

Research frontiers

Various alterations, such as activation of growth factor receptors, PI3K, catalytic, alpha polypeptide (PIK3CA) mutations and Epstein-Barr virus (EBV) infection lead to activation of the PI3K-Akt signaling pathway. However, clinicopathological and molecular correlates among such alterations have not been clearly addressed. In the present study, the authors identify new clinicopathological and molecular correlations between HER2 expression, PIK3CA mutations, EBV infection and phospho Akt (pAkt) expression in gastric cancer.

Innovations and breakthroughs

This is the first study to systematically characterize HER2 expression, PIK3CA mutations and EBV infection, all of which are involved in the PI3K-Akt signaling pathway, in a large cohort of patients with gastric cancer. The prevalence of these characteristics was thereby determined with a high level of precision and correlations with the clinicopathological and molecular features of gastric cancers, such as microsatellite instability and pAkt expression, could be assessed accurately for the first time.

Applications

The results have potentially important clinical implications since the mutational status of PIK3CA can be used to stratify cancer patients for genotype-based molecular therapies that target the HERs-PI3K pathway.

Terminology

PI3K-Akt pathway: Akt is believed to transduce the major downstream PI3K signals in cancer. Akt regulates cell growth and survival pathways by phosphorylating substrates such as GSK3, forkhead transcription factors, and the TSC2 tumor suppressor protein; PIK3CA: PIK3CA encodes a key enzymatic subunit of PI3K. Gain of function mutations in PIK3CA occur frequently in several cancer types. Hotspots of PIK3CA mutations are located in exons 9 and 20.

Peer review

The authors investigated HER2 expression, PIK3CA mutations and EBV infection in patients with gastric cancer. The results demonstrated that pAkt expression significantly correlates with the prognosis and the HER2 expression status in gastric cancer. This article is important for the further development of molecular targeted therapy in patients with advanced gastric cancer.

REFERENCES

1 **Hamilton JP**, Sato F, Greenwald BD, Suntharalingam M, Krasna MJ, Edelman MJ, Doyle A, Berki AT, Abraham JM, Mori Y, Kan T, Mantzur C, Paun B, Wang S, Ito T, Jin Z, Meltzer SJ. Promoter methylation and response to chemotherapy and radiation in esophageal cancer. *Clin Gastroenterol Hepatol* 2006; **4**: 701-708

2 **Tamura G**. Alterations of tumor suppressor and tumor-related genes in the development and progression of gastric

cancer. *World J Gastroenterol* 2006; **12**: 192-198
3 **Engelman JA**. Targeting PI3K signalling in cancer: opportunities, challenges and limitations. *Nat Rev Cancer* 2009; **9**: 550-562
4 **Mueller A**, Bachmann E, Linnig M, Khillimberger K, Schimanski CC, Galle PR, Moehler M. Selective PI3K inhibition by BKM120 and BEZ235 alone or in combination with chemotherapy in wild-type and mutated human gastrointestinal cancer cell lines. *Cancer Chemother Pharmacol* 2012; **69**: 1601-1615
5 **Bang YJ**, Van Cutsem E, Feyereislova A, Chung HC, Shen L, Sawaki A, Lordick F, Ohtsu A, Omuro Y, Satoh T, Aprile G, Kulikov E, Hill J, Lehle M, Rüschoff J, Kang YK. Trastuzumab in combination with chemotherapy versus chemotherapy alone for treatment of HER2-positive advanced gastric or gastro-oesophageal junction cancer (ToGA): a phase 3, open-label, randomised controlled trial. *Lancet* 2010; **376**: 687-697
6 **Sawaki A**, Ohashi Y, Omuro Y, Satoh T, Hamamoto Y, Boku N, Miyata Y, Takiuchi H, Yamaguchi K, Sasaki Y, Nishina T, Satoh A, Baba E, Tamura T, Abe T, Hatake K, Ohtsu A. Efficacy of trastuzumab in Japanese patients with HER2-positive advanced gastric or gastroesophageal junction cancer: a subgroup analysis of the Trastuzumab for Gastric Cancer (ToGA) study. *Gastric Cancer* 2012; **15**: 313-322
7 **Gravalos C**, Jimeno A. HER2 in gastric cancer: a new prognostic factor and a novel therapeutic target. *Ann Oncol* 2008; **19**: 1523-1529
8 **Hofmann M**, Stoss O, Shi D, Büttner R, van de Vijver M, Kim W, Ochiai A, Rüschoff J, Henkel T. Assessment of a HER2 scoring system for gastric cancer: results from a validation study. *Histopathology* 2008; **52**: 797-805
9 **Tanner M**, Hollmén M, Junttila TT, Kapanen AI, Tommola S, Soini Y, Helin H, Salo J, Joensuu H, Sihvo E, Elenius K, Isola J. Amplification of HER-2 in gastric carcinoma: association with Topoisomerase IIalpha gene amplification, intestinal type, poor prognosis and sensitivity to trastuzumab. *Ann Oncol* 2005; **16**: 273-278
10 **Samuels Y**, Wang Z, Bardelli A, Silliman N, Ptak J, Szabo S, Yan H, Gazdar A, Powell SM, Riggins GJ, Willson JK, Markowitz S, Kinzler KW, Vogelstein B, Velculescu VE. High frequency of mutations of the PIK3CA gene in human cancers. *Science* 2004; **304**: 554
11 **Lee JW**, Soung YH, Kim SY, Lee HW, Park WS, Nam SW, Kim SH, Lee JY, Yoo NJ, Lee SH. PIK3CA gene is frequently mutated in breast carcinomas and hepatocellular carcinomas. *Oncogene* 2005; **24**: 1477-1480
12 **Li VS**, Wong CW, Chan TL, Chan AS, Zhao W, Chu KM, So S, Chen X, Yuen ST, Leung SY. Mutations of PIK3CA in gastric adenocarcinoma. *BMC Cancer* 2005; **5**: 29
13 **Velho S**, Oliveira C, Ferreira A, Ferreira AC, Suriano G, Schwartz S, Duval A, Carneiro F, Machado JC, Hamelin R, Seruca R. The prevalence of PIK3CA mutations in gastric and colon cancer. *Eur J Cancer* 2005; **41**: 1649-1654
14 **Ligresti G**, Militello L, Steelman LS, Cavallaro A, Basile F, Nicoletti F, Stivala F, McCubrey JA, Libra M. PIK3CA mutations in human solid tumors: role in sensitivity to various therapeutic approaches. *Cell Cycle* 2009; **8**: 1352-1358
15 **Barbi S**, Cataldo I, De Manzoni G, Bersani S, Lamba S, Mattuzzi S, Bardelli A, Scarpa A. The analysis of PIK3CA mutations in gastric carcinoma and metanalysis of literature suggest that exon-selectivity is a signature of cancer type. *J Exp Clin Cancer Res* 2010; **29**: 32
16 **Kataoka Y**, Mukohara T, Shimada H, Saijo N, Hirai M, Minami H. Association between gain-of-function mutations in PIK3CA and resistance to HER2-targeted agents in HER2-amplified breast cancer cell lines. *Ann Oncol* 2010; **21**: 255-262
17 **Weidlich S**, Walsh K, Crowther D, Burczynski ME, Feuerstein G, Carey FA, Steele RJ, Wolf CR, Miele G, Smith G. Pyrosequencing-based methods reveal marked inter-individual differences in oncogene mutation burden in human colorectal tumours. *Br J Cancer* 2011; **105**: 246-254
18 **Kang GH**, Lee S, Kim WH, Lee HW, Kim JC, Rhyu MG, Ro JY. Epstein-barr virus-positive gastric carcinoma demonstrates frequent aberrant methylation of multiple genes and constitutes CpG island methylator phenotype-positive gastric carcinoma. *Am J Pathol* 2002; **160**: 787-794
19 **Kusano M**, Toyota M, Suzuki H, Akino K, Aoki F, Fujita M, Hosokawa M, Shinomura Y, Imai K, Tokino T. Genetic, epigenetic, and clinicopathologic features of gastric carcinomas with the CpG island methylator phenotype and an association with Epstein-Barr virus. *Cancer* 2006; **106**: 1467-1479
20 **Chang MS**, Uozaki H, Chong JM, Ushiku T, Sakuma K, Ishikawa S, Hino R, Barua RR, Iwasaki Y, Arai K, Fujii H, Nagai H, Fukayama M. CpG island methylation status in gastric carcinoma with and without infection of Epstein-Barr virus. *Clin Cancer Res* 2006; **12**: 2995-3002
21 **Hino R**, Uozaki H, Murakami N, Ushiku T, Shinozaki A, Ishikawa S, Morikawa T, Nakaya T, Sakatani T, Takada K, Fukayama M. Activation of DNA methyltransferase 1 by EBV latent membrane protein 2A leads to promoter hypermethylation of PTEN gene in gastric carcinoma. *Cancer Res* 2009; **69**: 2766-2774
22 **Gori S**, Sidoni A, Colozza M, Ferri I, Mameli MG, Fenocchio D, Stocchi L, Foglietta J, Ludovini V, Minenza E, De Angelis V, Crinò L. EGFR, pMAPK, pAkt and PTEN status by immunohistochemistry: correlation with clinical outcome in HER2-positive metastatic breast cancer patients treated with trastuzumab. *Ann Oncol* 2009; **20**: 648-654
23 **Nosho K**, Kawasaki T, Ohnishi M, Suemoto Y, Kirkner GJ, Zepf D, Yan L, Longtine JA, Fuchs CS, Ogino S. PIK3CA mutation in colorectal cancer: relationship with genetic and epigenetic alterations. *Neoplasia* 2008; **10**: 534-541
24 **Baba Y**, Nosho K, Shima K, Hayashi M, Meyerhardt JA, Chan AT, Giovannucci E, Fuchs CS, Ogino S. Phosphorylated AKT expression is associated with PIK3CA mutation, low stage, and favorable outcome in 717 colorectal cancers. *Cancer* 2011; **117**: 1399-1408
25 **Rudd ML**, Price JC, Fogoros S, Godwin AK, Sgroi DC, Merino MJ, Bell DW. A unique spectrum of somatic PIK3CA (p110alpha) mutations within primary endometrial carcinomas. *Clin Cancer Res* 2011; **17**: 1331-1340
26 **Miyake T**, Yoshino K, Enomoto T, Takata T, Ugaki H, Kim A, Fujiwara K, Miyatake T, Fujita M, Kimura T. PIK3CA gene mutations and amplifications in uterine cancers, identified by methods that avoid confounding by PIK3CA pseudogene sequences. *Cancer Lett* 2008; **261**: 120-126
27 **Oda K**, Okada J, Timmerman L, Rodriguez-Viciana P, Stokoe D, Shoji K, Taketani Y, Kuramoto H, Knight ZA, Shokat KM, McCormick F. PIK3CA cooperates with other phosphatidylinositol 3'-kinase pathway mutations to effect oncogenic transformation. *Cancer Res* 2008; **68**: 8127-8136
28 **Gymnopoulos M**, Elsliger MA, Vogt PK. Rare cancer-specific mutations in PIK3CA show gain of function. *Proc Natl Acad Sci USA* 2007; **104**: 5569-5574
29 **Corso G**, Velho S, Paredes J, Pedrazzani C, Martins D, Milanezi F, Pascale V, Vindigni C, Pinheiro H, Leite M, Marrelli D, Sousa S, Carneiro F, Oliveira C, Roviello F, Seruca R. Oncogenic mutations in gastric cancer with microsatellite instability. *Eur J Cancer* 2011; **47**: 443-451
30 **Berns K**, Horlings HM, Hennessy BT, Madiredjo M, Hijmans EM, Beelen K, Linn SC, Gonzalez-Angulo AM, Stemke-Hale K, Hauptmann M, Beijersbergen RL, Mills GB, van de Vijver MJ, Bernards R. A functional genetic approach identifies the PI3K pathway as a major determinant of trastuzumab resistance in breast cancer. *Cancer Cell* 2007; **12**: 395-402
31 **Wang L**, Zhang Q, Zhang J, Sun S, Guo H, Jia Z, Wang B, Shao Z, Wang Z, Hu X. PI3K pathway activation results in low efficacy of both trastuzumab and lapatinib. *BMC Cancer*

2011; **11**: 248

32 **Crawford A**, Nahta R. Targeting Bcl-2 in Herceptin-Resistant Breast Cancer Cell Lines. *Curr Pharmacogenomics Person Med* 2011; **9**: 184-190

33 **Murakami D**, Tsujitani S, Osaki T, Saito H, Katano K, Tatebe S, Ikeguchi M. Expression of phosphorylated Akt (pAkt) in gastric carcinoma predicts prognosis and efficacy of chemotherapy. *Gastric Cancer* 2007; **10**: 45-51

34 **Oki E**, Baba H, Tokunaga E, Nakamura T, Ueda N, Futatsugi M, Mashino K, Yamamoto M, Ikebe M, Kakeji Y, Maehara Y. Akt phosphorylation associates with LOH of PTEN and leads to chemoresistance for gastric cancer. *Int J Cancer* 2005; **117**: 376-380

35 **Rojo F**, Tabernero J, Albanell J, Van Cutsem E, Ohtsu A, Doi T, Koizumi W, Shirao K, Takiuchi H, Ramon y Cajal S, Baselga J. Pharmacodynamic studies of gefitinib in tumor biopsy specimens from patients with advanced gastric carcinoma. *J Clin Oncol* 2006; **24**: 4309-4316

36 **Min Y**, Adachi Y, Yamamoto H, Imsumran A, Arimura Y, Endo T, Hinoda Y, Lee CT, Nadaf S, Carbone DP, Imai K. Insulin-like growth factor I receptor blockade enhances chemotherapy and radiation responses and inhibits tumour growth in human gastric cancer xenografts. *Gut* 2005; **54**: 591-600

S- Editor Gou SX **L- Editor** A **E- Editor** Li JY

Gut Online First, published on November 20, 2012 as 10.1136/gutjnl-2011-301746

ORIGINAL ARTICLE

Treatment of pancreatic fibrosis with siRNA against a collagen-specific chaperone in vitamin A-coupled liposomes

Hirotoshi Ishiwatari,[1] Yasushi Sato,[1] Kazuyuki Murase,[1] Akihiro Yoneda,[2] Ryosuke Fujita,[2] Hiroki Nishita,[2] Naoko Kubo Birukawa,[2] Tsuyoshi Hayashi,[1] Tsutomu Sato,[1] Koji Miyanishi,[1] Rishu Takimoto,[1] Masayoshi Kobune,[1] Shigenori Ota,[3] Yasutoshi Kimura,[3] Koichi Hirata,[3] Junji Kato,[1] Yoshiro Niitsu[2]

► Additional supplementary files are published online only. To view these files please visit the journal online (http://dx.doi.org/10.1136/gutjnl-2011-301746).

[1]Fourth Department of Internal Medicine, Sapporo Medical University, Sapporo, Japan
[2]Department of Molecular Target Exploration, Sapporo Medical University, Sapporo, Japan
[3]First Department of Surgery, Sapporo Medical University, Sapporo, Japan

Correspondence to
Professor Yoshiro Niitsu, Department of Molecular Target Exploration, Sapporo Medical University School of Medicine, South 1, West 17, Chuo-ku, Sapporo 060-8543, Japan; niitsu@sapmed.ac.jp

HI, YS and KM contributed equally to this work.

Revised 27 September 2012
Accepted 12 October 2012

ABSTRACT

Background and objective Fibrosis associated with chronic pancreatitis is an irreversible lesion that can disrupt pancreatic exocrine and endocrine function. Currently, there are no approved treatments for this disease. We previously showed that siRNA against collagen-specific chaperone protein gp46, encapsulated in vitamin A-coupled liposomes (VA-lip-siRNAgp46), resolved fibrosis in a model of liver cirrhosis. This treatment was investigated for pancreatic fibrosis induced by dibutyltin dichloride (DBTC) and cerulein in rats.

Methods Specific uptake of VA-lip-siRNAgp46, conjugated with 6′-carboxyfluorescein (FAM) by activated pancreatic stellate cells (aPSCs), was analysed by fluorescence activated cell sorting (FACS). Intracellular distribution of VA-lip-siRNAgp46-FAM was examined by fluorescent microscopy. Suppression of gp46 expression by VA-lip-siRNAgp46 was assessed by immunoblotting. Collagen synthesis in aPSCs was assayed by dye-binding. Specific delivery of VA-lip-siRNAgp46 to aPSCs in DBTC rats was verified following intravenous VA-lip-siRNA-FAM and ^{3}H-VA-lip-siRNAgp46. The effect of VA-lip-siRNA on pancreatic histology in DBTC- and cerulein-treated rats was determined by Azan-Mallory staining and hydroxyproline content.

Results FACS analysis revealed specific uptake of VA-lip-siRNAgp46-FAM through the retinol binding protein receptor by aPSCs in vitro. Immunoblotting and collagen assay verified knockdown of gp46 and suppression of collagen secretion, respectively, by aPSCs after transduction of VA-lip-siRNAgp46. Specific delivery of VA-lip-siRNAgp46 to aPSCs in fibrotic areas in DBTC rats was confirmed by fluorescence and radioactivity 24 h after the final injection. 10 systemic VA-lip-siRNAgp46 treatments resolved pancreatic fibrosis, and suppressed tissue hydroxyproline levels in DBTC- and cerulein-treated rats.

Conclusion These data suggest the therapeutic potential of the present approach for reversing pancreatic fibrosis.

Significance of this study

What is already known on this subject?
- Pancreatic fibrosis is an irreversible lesion that can disrupt pancreatic function; there are no approved treatments.
- The accumulation of fibrotic tissue results from sustained activation of pancreatic stellate cells (PSCs).
- The characteristics of PSCs resemble those of hepatic stellate cells (HSCs).
- We have previously succeeded in resolving liver fibrosis in cirrhotic rat models by targeting HSCs with vitamin A coupled liposomes which carried siRNA against the collagen specific chaperone protein gp46.

What are the new findings?
- Rat activated PSCs take up vitamin A-coupled liposomes (VA-lip-siRNAgp46) in a retinol binding protein-mediated fashion, similarly to activated HSCs.
- Transduction of siRNAgp46 in activated PSCs caused suppression of collagen secretion.
- Activated PSCs specifically took up siRNAgp46 encapsulated in vitamin A liposomes in the pancreas of dibutyltin dichloride (DBTC)-treated rats.
- VA-lip-siRNAgp46 treatments resolved pancreatic fibrosis, and suppressed tissue hydroxyproline levels in DBTC- and cerulein-treated rats.
- This is the first demonstration of successful targeting of antifibrotic drug to both cells and molecule which are responsible for pancreatic fibrosis.

How might it impact on clinical practice in the foreseeable future?
- Results suggest the therapeutic potential of the present approach for reversing pancreatic fibrosis.

INTRODUCTION

Chronic pancreatitis is characterised by inflammation and replacement of parenchymal cells with fibrotic tissue leading to functional alterations, such as debilitating exocrine and occasional endocrine insufficiency. The accumulation of fibrotic tissue results from sustained activation of pancreatic stellate cells (PSCs), which proliferate and secrete collagen in response to stimulation by cytokines, growth factors, and reactive oxygen species from inflammatory cells and damaged pancreatic tissue.[1 2] Various approaches to suppress the

activation of PSCs and to eradicate activated PSCs (aPSCs) have been explored for the prevention and treatment of fibrosis associated with chronic pancreatitis.[3–5] However, so far no clinically applicable agents have been developed, mainly because of the inability for specific drug delivery to aPSCs.

We previously demonstrated complete resolution of liver cirrhosis in rat models using vitamin A-coupled liposomes to specifically deliver siRNA against the collagen-specific chaperone, gp46 (VA-lip-siRNAgp46), to hepatic stellate cells (HSCs) via the circulating receptor for retinol binding protein (RBP).[6] The characteristics of PSCs, including collagen synthesis, storage of vitamin A, expression of gp46, etc, resemble those of HSCs.[7] Therefore, in the present study, we examined whether our previous therapeutic approach for liver cirrhosis could be successfully applied for the treatment of pancreatic fibrosis.

MATERIALS AND METHODS

Preparation of siRNAgp46 and its conjugate with 6′-carboxyfluorescein

A formulation of siRNA directed against gp46, a rat homologue of human HSP47, was purchased from Hokkaido System Science (Sapporo, Japan). The sense and anti-sense strands of siRNAs have been described in detail previously.[6] For fluorescence activated cell sorting (FACS) analyses and in vivo tracing of gp46siRNA, gp46 siRNA with 6′-carboxyfluorescein (6-FAM) -coupled to the 5′ end of the sense strand was used.

A formulation of siRNA directed against HSP47 (GenBank accession no. 50454) was purchased from Hokkaido System Science. The sense and anti-sense strands of siRNAs were: HSP47, 5′-ggacaggccucuac aacuaTT-3′ (sense); 5′-uaguuguagagg ccuguccTT-3′ (antisense).

Preparation of vitamin A-coupled liposomes carrying siRNAgp46

Vitamin A-coupled liposomes carrying siRNAgp46 (VA-lip-siRNAgp46) were prepared as described previously.[6]

Animals

Male Lewis rats (Charles River, Tokyo, Japan), weighing 150–200 g, and male Wistar rats (Charles River), weighing 250–300 g, were used for dibutyltin dichloride (DBTC) and cerulein experiments, respectively. All animal procedures were approved by the Sapporo Medical College Institutional Animal Care and Use Committee.

Isolation and cultivation of rat PSCs

Rat PSCs were isolated by density gradient centrifugation, as detailed previously.[8] All experiments were performed with culture-activated cells (aPSCs, passage 1–3).

Isolation and cultivation of human PSCs

Human pancreases were obtained during surgery for chronic pancreatitis. All these patients were seen at Sapporo Medical University. Informed consent in writing was obtained from each patient. Human PSCs were isolated by outgrowth, using explant techniques from the pancreas as described previously.[1] In this study, experiments were performed on activated α-smooth muscle actin (SMA)-positive cells between the first and third serial passages using lines.

FACS analysis of VA-lip-siRNAgp46-FAM

Rat aPSCs were cultivated with VA-lip-siRNAgp46-FAM (50 nM of siRNA) for 30 min. For the blocking assay, 1×10^4 cells were treated with mouse anti-RBP antibody (10 μg/ml, BD Pharmingen, San Diego, California, USA) for 30 min before adding VA-lip-siRNAgp46-FAM. The mean fluorescence intensity of VA-lip-siRNAgp46-FAM-treated cells was assessed on a FACScalibur with CellQuest software (Becton Dickinson, San Jose, California, USA).

Intracellular distribution analysis of VA-lip-siRNAgp46-FAM

Distribution of VA-lip-siRNAgp46-FAM in aPSCs after transduction was analysed as described previously.[6]

Western blot analysis

Protein extracts of cells and pancreas specimens were resolved over 4/20 sodium dodecylsulphate–polyacrylamide gels, transferred onto nitrocellulose membranes, probed with antibodies against HSP47 (gp46) (Stressgen Biotechnologies, Victoria, BC, Canada) or β-actin (Cell Signaling, Beverly, Massachusetts, USA), and then probed with peroxidase-coupled antibodies as the secondary antibody (Oncogene Research Product, Boston, Massachusetts, USA). Lastly, the cells were visualised with ECL (Amersham Life Science, Arlington Heights, Illinois, USA). Western blots were quantified using ImageJ 1.43u (NIH, Bethesda, Maryland, USA).

Quantification of collagen production

Collagen production by rat aPSCs was measured according to the method described previously for aHSCs, except for cell cultivation period after transduction; 24 h for aHSCs and 72 h for aPSCs.[6 9]

Quantitative RT–PCR

Total RNA was isolated using RNeasy mini kits (Qiagen, Hilden, Germany). Total RNA (1 μg) was used for reverse transcription with SuperScript II (Invitrogen, Carlsbad, California, USA) plus RNaseOUT (Invitrogen) using random primers (Invitrogen) according to the manufacturer's instructions. All TaqMan primers mixed with probes (GAPDH, Rn 99999916_s1; MMP2, Rn 02532334_s1; COL1A1, Rn00801649_g1; TIMP-1, Rn 00587558_m1; Gp46, Rn 00367777_m1; TGFβ, Rn01475963_m1) were purchased from Applied Biosystems (Foster City, California, USA). The TaqMan reactions were performed using 7300 Fast Real Time PCR System (Applied Biosystems). The results were expressed as the ratio of the number of copies of the product gene to the number of copies of the housekeeping gene (GAPDH) from the same RNA (respective cDNA) sample and PCR run.

Induction of pancreatic and hepatic fibrosis by DBTC

Among several models of pancreatic fibrosis,[10–18] we chose the DBTC model in which the common bile duct is obstructed by a plug formed with necrotic biliopancreatic ductal epithelium, because the procedure is relatively simple to perform as compared with other models and irreversible pancreatitis can be induced by a single injection of DBTC. DBTC (Sigma, St Louis, Missouri, USA) was first dissolved in ethanol (1 part) and then mixed with glycerol (2 parts) and dimethyl sulfoxide (2 parts).[10] For administration of DBTC, we selected the right jugular vein route to avoid any possible damage of the tail vein caused by the tail vein route for subsequent application of VA-lip-siRNAgp46.[10] In preliminary experiments, we found the lethality rates of dosages 8.0, 7.0 and 5.0 mg/kg body weight to be 4/4 (100%), 7/16 (44%) and 5/27 (19%), respectively. Thus, we selected the dosage of 5.0 mg/kg for the main experiments (see online supplementary figure S1).

Fibrosis, as revealed by Azan-Mallory staining, was evident in pancreatic and hepatic specimens on days 29 and 43 of DBTC injection (see online supplementary figure S1A–C).

Induction of pancreatic fibrosis by cerulein

Male Wistar rats received two intraperitoneal injections of 50 μg/kg cerulein (Sigma) 1 h apart every week for 6 weeks, as described by Ishibashi (see online supplementary figure S2A,B).[18]

Collagenase activity in pancreas homogenates

Collagenase activity (collagen type I) in pancreas homogenates was measured as described previously.[19]

In vivo localisation of VA-lip-siRNArandom-FAM in rat pancreas

From day 43 of DBTC administration, rats were injected intravenously with 1 μl/g body weight of VA-lip-siRNArandom-FAM or Lip-siRNArandom-FAM (0.75 mg/kg siRNA) three times on alternating days. At 24 h after the last injection, the rats were sacrificed by saline perfusion. Pancreatic tissue was immediately embedded in OCT compound (Sakura Finetechnical, Tokyo, Japan) medium and cryogenically sectioned. Multicoloured fluorescent staining of sections and their analysis were carried out as described previously.[6]

Tissue distribution of radiolabelled VA-lip-siRNArandom

^{3}H-VA-lip-siRNArandom (200 μCi), prepared as described previously, was administered via the tail vein under normal pressure in either DBTC-treated rats (day 43) or normal rats. After 24 h, the rats were sacrificed under anaesthesia, and radioactivity of each tissue was assayed as described previously.[6]

Treatment of DBTC rats and cerulein rats with VA-lip-siRNAgp46 and measurement of hydroxyproline content

Three groups of rats (n=10 per group) were used for histological evaluations. From day 43 of DBTC or cerulein administration, Lip-siRNAgp46, VA-lip-siRNAgp46 (0.75 mg/kg siRNA) or phosphate buffered saline (PBS; three times a week every other day) were injected for a total of 10 times via the tail vein under normal pressure in a volume of 1 μl/g body weight.[6] Hydroxyproline content in the pancreas was measured as previously described.[20]

Immunohistochemical staining for α-SMA

Pancreas was fixed with 10% paraformaldehyde. Then, immunohistochemical staining for α-SMA was performed by the dextran polymer method using monoclonal anti α-SMA antibody (1 : 1000, Sigma) and an Envision Kit (Dako), followed by colouring with 3, 3'-diaminobenzidine (DAB) and nuclear staining with Gill's haematoxylin solution. To accurately quantitate areas stained with α-SMA, slides from six randomly selected low-power fields (×100) per pancreas section from each rat were viewed by microscopy (Axioplan 2; Carl Zeiss) and the percentage of areas stained with α-SMA was quantified as previously described.[6]

In vitro apoptosis assay

Rat and human aPSCs under going apoptosis were stained with an in situ Cell Death Detection kit (Roche) according to the manufacturer's protocol. Slides were washed with PBS, and exposed to Prolong Gold Antifade Reagent with 4', 6-diamidino-2-phenylindole (DAPI) (Molecular Probes) to stain nuclei. The number of terminal deoxynucleotidyl transferase-mediated deoxyuridine triphosphate nick-end labelling (TUNEL)-positive cells (green) in aPSCs were counted in 10 random high-power fields (×800) using fluorescent microscopy (Keyence, BZ-8000) for each sample.

Double staining of pancreas specimen for TUNEL and α-SMA

Double staining for TUNEL and α-SMA was undertaken and the number of TUNEL-positive apoptotic cells within the fibrotic bands was determined using a method modified from that described by Iredale *et al*.[19] Briefly, the specimen was first stained with an in situ Cell Death Detection kit (Roche) according to the manufacturer's protocol, followed by immunostaining for α-SMA (Sigma), with an alkaline phosphatase-conjugated anti-mouse second antibody (KPL, Gaithersburg, Maryland, USA) using a Vector Red alkaline phosphatase substrate kit 1 (Vector Lab, Peterborough, UK). The number of TUNEL-positive cells (brown) in α-SMA-positive areas (red), but not those in parenchymal area, were counted in 10 random high-power fields (×800).

Ethics approval

This research follows the tenets and regulations of the Declaration of Helsinki and has been approved by the Animal Care and the Institutional Review Board at Sapporo Medical University.

Statistics

Results are presented as mean±SD for each sample. Multiple comparisons between control groups and other groups were performed by Dunnet's test.

RESULTS

Specific uptake of RBP bound VA-lip-siRNAgp46 by rat aPSCs

Rat aPSCs, which were stained positive for α-SMA (figure 1A), were incubated with VA-lip-siRNAgp46-FAM or Lip-siRNAgp46-FAM in the presence of 10% fetal calf serum, and were observed under a fluorescence microscope. In VA-lip-siRNAgp46-FAM treated aPSCs, fluorescence appeared as a fine granular pattern in the cytoplasm at 30 min and as denser granular patterns in the perinuclear region at 2 h (figure 1B). In contrast, in Lip-siRNAgp46-FAM treated aPSCs, no green fluorescence was seen at 30 min and perinuclear fluorescence at 2 h was very faint (figure 1B). The fluorescence intensity of VA-lip-siRNAgp46-FAM aPSCs as revealed by FACS was clearly suppressed by RBP antibody to nearly the same level as Lip-siRNAgp46-FAM aPSCs (figure 1C).

Suppression of gp46 expression and collagen secretion of rat aPSCs by VA-lip-siRNAgp46

Treatment of aPSCs with VA-lip-siRNAgp46 brought about dose-dependent suppression of gp46 with almost complete suppression at 50 nM, which lasted at least 72 h (figure 1D,E) while treatment with VA-lip-siRNA random or Lip-siRNAgp46 did not cause any suppression. In the culture plate of VA-lip-siRNAgp46-treated aPSCs, significantly less collagen than that of VA-lip-siRNA random-treated or non-treated aPSCs was found (figure 1F).

Delivery of VA-lip-siRNArandom-FAM to aPSCs in vivo

The specific delivery of VA-lip-siRNArandom-FAM to aPSCs in the fibrotic pancreas was examined by fluorescent emission 24 h after three injections (figure 2A). Specimens were prepared from head (figure 2B,D) and body portions (figure 2C,E) of the pancreas. In both portions, fluorescence of VA-lip-siRNArandom-FAM (green) was identified predominantly in the

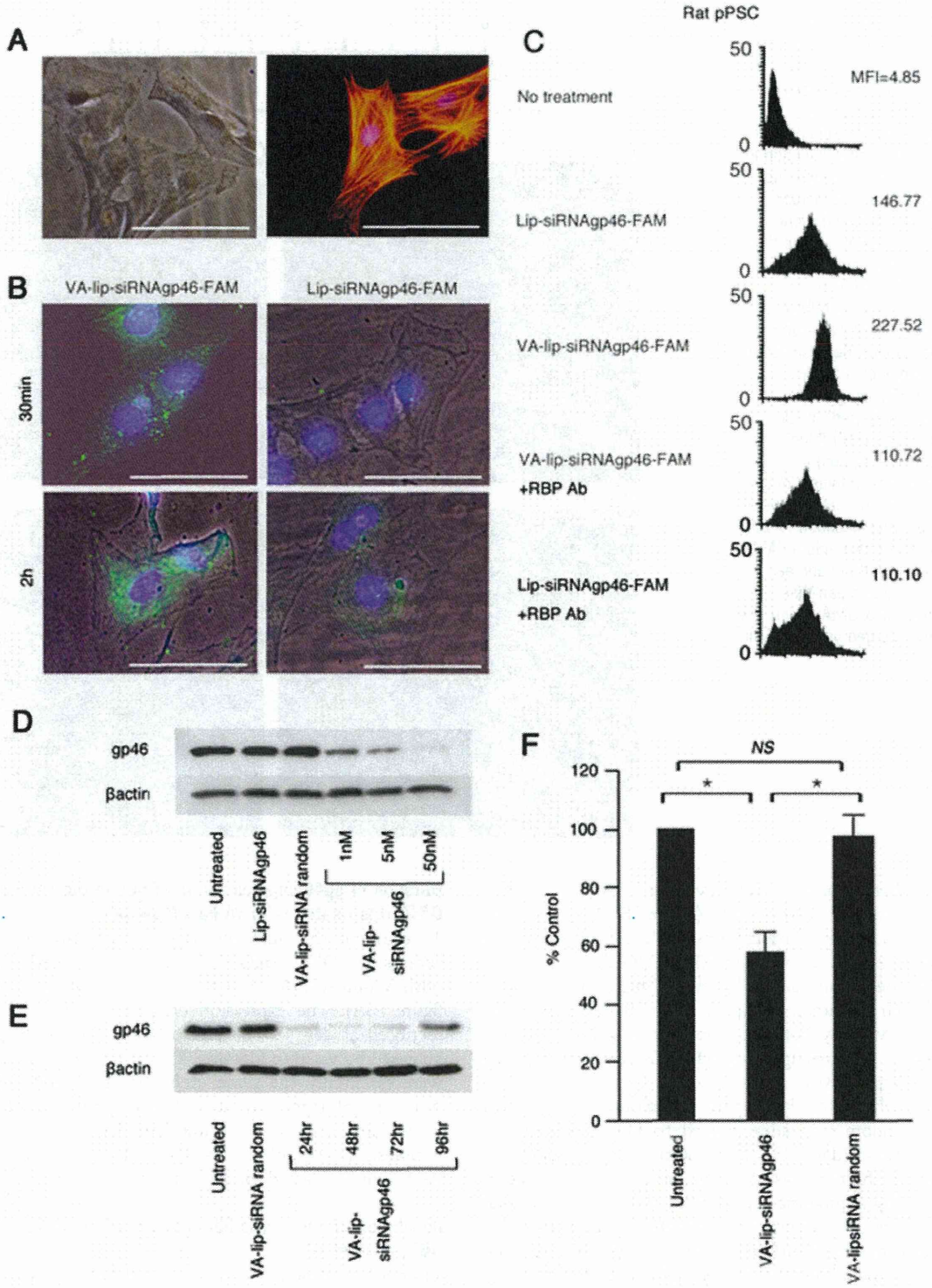

Figure 1 Retinol binding protein receptor-dependent uptake of vitamin A-coupled liposomes (VA-lip-siRNAgp46)-carboxyfluorescein (FAM) by activated pancreatic stellate cells (aPSCs) and suppressive effect of siRNAgp46 on gp46 expression and collagen synthesis. (A) Representative fluorescent images of rat aPSCs. Phase-contrast micrograph image of aPSCs (left panel) and immunofluorescent staining of aPSCs with Cy3-conjugated anti-α-SMA antibody (red) and nuclei counterstained with DAPI (blue) (right panel). Bars=100 μm. (B) Representative fluorescent images of the intracellular distribution of FAM-labelled siRNA. Rat aPSCs were treated with VA-lip-siRNAgp46-FAM or Lip-siRNAgp46-FAM. At 30 min, the medium was replaced with fresh medium. At the time indicated, cells were fixed and analysed by fluorescence microscopy to determine the relative intracellular distribution of siRNA-FAM (green). Bars=100 μm. One of five representative images is shown. (C) Representative fluorescence activated cell sorting patterns of rat PSCs treated with vitamin A-free liposomes carrying siRNAgp46-FAM (Lip-siRNAgp46-FAM) or VA-lip-siRNAgp46-FAM with or without anti-RBP antibody. Mean fluorescence intensity is indicated. Five independent experiments were carried out in each set of aPSCs and the results were essentially the same. (D) Western blotting was used to analyse the expression of gp46 and β-actin

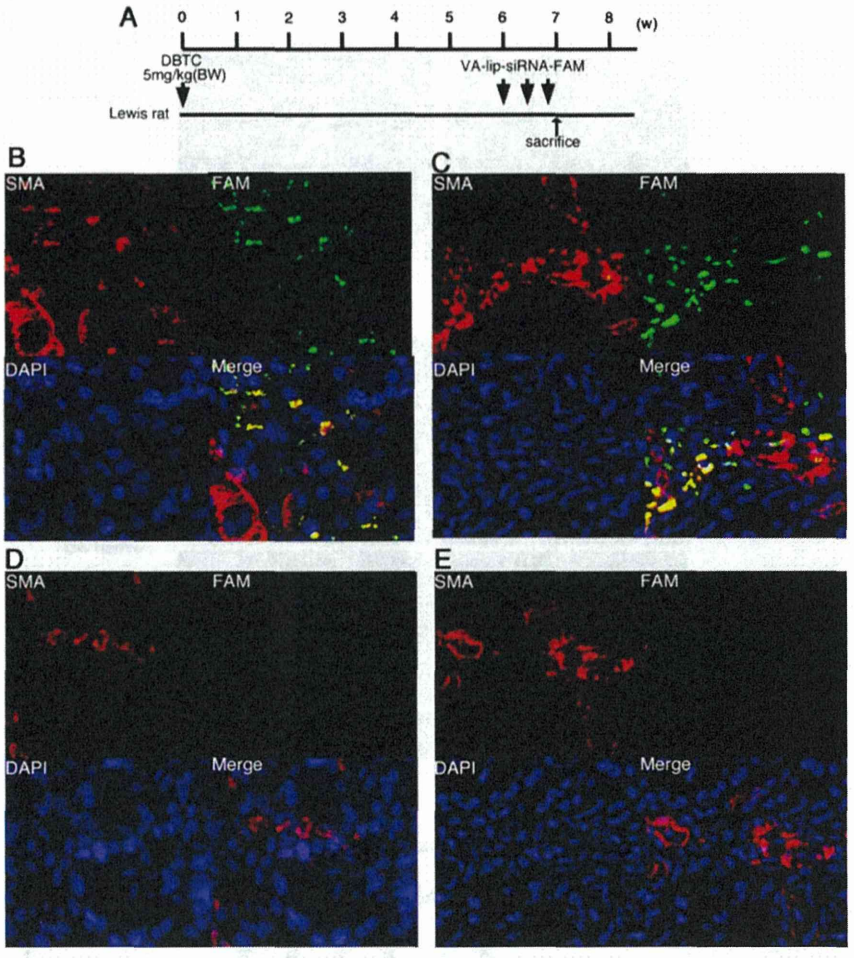

Figure 2 Specific delivery of vitamin A-coupled liposomes(VA-lip-siRNA) random-carboxyfluorescein (FAM) to activated pancreatic stellate cells (aPSCs) in dibutyltin dichloride (DBTC)-treated rats. (A) Schedule of VA-lip-siRNArandom-FAM injection in rats with DBTC-induced pancreatic fibrosis. Samples (B, D; pancreas head, C, E; pancreas body) were obtained from DBTC-treated rats that received three injections of VA-lip-siRNArandom-FAM or Lip-siRNArandom-FAM (siRNA doses of 0.75 mg/kg, 3 times every other day) (n=6 per group). Representative fluorescent images of α-SMA visualised by Cy3-conjugated anti-α-SMA antibody (red), nuclei counterstained with DAPI (blue) and siRNA random-FAM (green) in pancreas specimens obtained 24 h after the last injection. Pictures were taken at original magnification (×200). Fluorescence of siRNA random-FAM (green) was identified in pancreas, predominantly in the region that stained positive for α-SMA giving rise to areas with a merged yellow colour.

spotty region that stained positive only for α-SMA (aPSCs) (red), giving rise to a merged yellow colour (figure 2B,C). By contrast, in rats treated with Lip-siRNArandom-FAM, the yellow area in α-SMA positive regions was negligible (figure 2D,E).

The yellow area in six randomly selected high-power (×200) fields from each specimen occupied 32.1±10.5% of the area stained for α-SMA. By contrast, the yellow area in α-SMA-positive regions was negligible (2.0±1.5%) in a rat injected with lip-siRNAgp46-FAM.

To further elucidate the organ distribution, ^{3}H-labelled VA-lip-siRNArandom was administered to DBTC-treated rats with pancreatitis (day 43) and normal rats (table 1). Radioactivity in the pancreas of DBTC-treated rats was significantly higher (by approximately fivefold) than that of normal rats. In the liver, radioactivity in the DBTC group was also higher (approximately fourfold) than that of normal rats. Other organs, including the lungs, spleen and intestines, showed no increase in radioactivity in DBTC-treated rats, relative to normal rats.

Duration of gp46 suppression in aPSCs in the pancreas of DBTC rats treated with VA-lip-siRNAgp46

To examine the duration of effect of siRNAgp46 on gp46 expression, DBTC rats (n=15) were injected intravenously with VA-lip-siRNAgp46 on day 43 (see online supplementary figure S3A). The expression of gp46 in the pancreas of rats sacrificed at day 43, 44, 45, 46 and 47 (n=3 per group), was analysed by western blotting. The results for each rat per group were essentially the same. Representative western blot bands from one of three rats at each time-point and densitometric values are shown in online supplementary figure S3B,C. Suppression of gp46 expression started 24 h after initiated of treatment and lasted for at least 3 days.

Resolution of pancreatic fibrosis by VA-lip-siRNAgp46 in DBTC-treated rats

After 10 treatments with VA-lip-siRNAgp46 (figure 3A), an apparent reduction and statistically significant reduction analysed by computerised imaging of fibrosis represented by

(normalisation control) in aPSCs transfected with Lip-siRNAgp46,VA-lip-siRNA random or VA-lip-siRNAgp46. Dose-dependent inhibition of gp46 expression by siRNAgp46 was observed. (E) Duration of suppressive effect of siRNAgp46 on gp46 expression in aPSCs. Rat aPSCs were treated with VA-lip-siRNAgp46 or VA-lip-siRNA random. At 30 min, the medium was replaced with fresh medium. At the time indicated, the expression of gp46 and β-actin (normalisation control) was analysed by western blotting. Similar results were obtained in three independent experiments. (F) Collagen deposition on tissue culture plates was assayed by the dye-binding method 72 h after transduction in rat aPSCs treated with VA-lip-siRNAgp46 or with VA-lip-siRNArandom. Data are expressed as mean±SD calculated from five transductions and as a percentage of untreated control. *p<0.05 vs VA-lip-siRNAgp46. NS, not significant.

Table 1 Tissue biodistribution of (^{3}H)VA-lip-siRNAgp46 in rats

	Radioactivity (cpm/tissue)			
	Normal ($\times10^5$)	DBTC rat ($\times10^5$)	p Value (normal vs DBTC rat)	Ratio (DBTC rat/ normal)
Pancreas	0.481±0.270	2.42±0.840	0.001	5.03
Liver	77.2±21.0	319±105	0.002	4.14
Lung	3.83±1.89	5.26±3.66	NS	1.37
Spleen	1.75±0.740	1.84±1.11	NS	1.05
Intestine	4.23±1.59	4.52±1.00	NS	1.07

DBTC-treated rats (day 43 rat) and normal rats (n=3 per group) received a single intravenous injection of 200 μCi (^{3}H)VA-lip-siRNAgp46 via the tail vein. Tissue biodistribution was analysed 24 h later. Data represent means±SD (n=3). Similar results were obtained in two independent experiments.
DBTC, dibutyltin dichloride; NS, not significant; VA-lip-siRNAgp46, vitamin A-coupled liposomes.

Azan-Mallory positive area was confirmed (figure 3B,C). Results were consistent with data showing substantial suppression of hydroxyproline levels (figure 3D).

Disappearance of aPSCs following treatment with VA-lip-siRNAgp46

To elucidate of disappearance of aPSCs after treatment, immunostaining for α-SMA was performed. A substantially smaller area was stained for α-SMA in rats treated with VA-lip-siRNAgp46 compared to the stained area in rats treated with Lip-siRNAgp46 or PBS (figure 3E,F).

Effect of VA-lip-siRNAgp46 treatment on pancreatic inflammation in DBTC-treated rats

Since it is known that PSCs play a role not only in fibrosis but also in the inflammatory response,[21] we explored the effect of VA-lip-siRNAgp46 treatment on inflammation of pancreas in DBTC-treated rats. The degree of inflammation, assessed by cell infiltration, fatty change, tubular complex formation and infiltration of macrophages and T cells were reduced after treatment with VA-lip-siRNAgp46 (see online supplementary figure S4 and table S1).

Resolution of hepatic fibrosis by VA-lip-siRNAgp46 in DBTC-treated rats

In the DBTC model, hepatic fibrosis occurs in addition to pancreatic fibrosis because DBTC causes obstruction of the common bile duct (see online supplementary figure S5A,B). The Azan-Mallory positive area was significantly reduced in specimens from VA-lip-siRNAgp46-treated rats as compared with that in control specimens (see online supplementary figure S5C).

Apoptosis of siRNAgp46-induced aPSCs

We examined the possibility that apoptotic death of rat aPSCs may be induced by siRNAgp46 treatment in vitro. The number of TUNEL positive cells was greater in siRNAgp46-transfected aPSCs than in control aPSCs (figure 4A). The ratio of apoptotic nuclei to total nuclei of siRNAgp46-transfected aPSCs was 38.3±8.2% and was significantly increased relative to controls (figure 4B).

Apoptosis of aPSCs by siRNAHSP47 was also examined in human PSCs obtained by outgrowth from fibrotic human pancreas. TUNEL staining in apoptotic nuclei of siRNAHSP47-transfected aPSCs was higher than in control aPSCs (figure 4C). The ratio of apoptotic nuclei to total nuclei of siRNAHSP47-transfected aPSCs was 18.3±4.2% and was significantly increased relative to controls (figure 4D).

Furthermore, apoptosis of aPSCs by siRNAgp46 was examined in DBTC-treated rats. In DBTC pancreas, TUNEL positive cells in areas overlapping with aPSCs (α-SMA positive) also increased after treatment with VA-lip-siRNAgp46 (figure 4E,F).

Resolution of pancreatic fibrosis by VA-lip-siRNAgp46 in cerulein-treated rats

In the cerulein induced pancreatitis model (see online supplementary figure S2 and figure 5A), the therapeutic effect of VA-lip-siRNAgp46 was also evident with respect to shrinkage of the fibrotic area (figure 5B) and suppression of hydroxyproline levels (figure 5C).

Changes in mRNA expression of fibrosis-related proteins before and after administration of VA-lip-siRNAgp46 in DBTC-treated rats

We measured mRNA levels of gp46, collagen I, MMP2, TIMP-1, and TGFβ in pancreas homogenates from normal rats and DBTC-treated rats (figure 6A). The mRNA ratios relative to GAPDH mRNA are shown in figure 6B. mRNAs of gp46, collagen I, MMP2 and TGFβ expressed in aPSCs were increased in fibrotic pancreas as compared to normal pancreas. TIMP-1 mRNA levels did not increase but instead showed a slight decrease in response to induction of fibrosis. However, after treatment with VA-lip-siRNAgp46, the expression of all mRNAs was significantly decreased, presumably due to the disappearance of aPSCs.

Elevated collagenase activity in the pancreas of DBTC-treated rats

To confirm that sufficient collagenase activity to resolve the predeposited collagen resides in fibrotic pancreas, we measured collagenase activity in the pancreas homogenates of DBTC-treated rats after three injections of VA-lip-siRNAgp46 (day 49), and found that it was significantly higher than that of control normal rat and became even higher after treatment with VA-lip-siRNA gp46 (figure 6C).

Changes in microvessel density in fibrotic pancreas tissue before and after treatment with VA-lip-siRNAgp46

In DBTC-treated pancreas before VA-lip-siRNAgp46 treatment, the mean microvessel counts were 39±9.5. After 10 injections of VA-lip-siRNAgp46, the mean microvessel counts significantly reduced to 19±9.2 (see online supplementary figure S6).

DISCUSSION

PSCs have been shown to store vitamin A and synthesise collagen, and they can be activated by inflammatory cytokines, exerting functions similar to those of HSCs.[1 2 7] However, it has not been elucidated whether RBP is involved in vitamin A uptake. It is also not clear whether HSP47 is involved in collagen secretion by aPSCs. Therefore we first clarified that aPSCs indeed take up vitamin A in an RBP-mediated fashion by demonstrating that with VA-lip-siRNAgp46-FAM, but not with Lip-siRNAgp46-FAM, the fluorescence that appeared within 30 min of incubation was suppressed by anti-RBP antibody, and the amount of collagen on the culture plate of VA-lip-siRNAgp46-treated cells was significantly reduced (figure 1C,F). These findings verified the similarity of aPSCs to activated hepatic stellate cells in terms of RBP-mediated vitamin A uptake and gp46 -assisted collagen secretion.

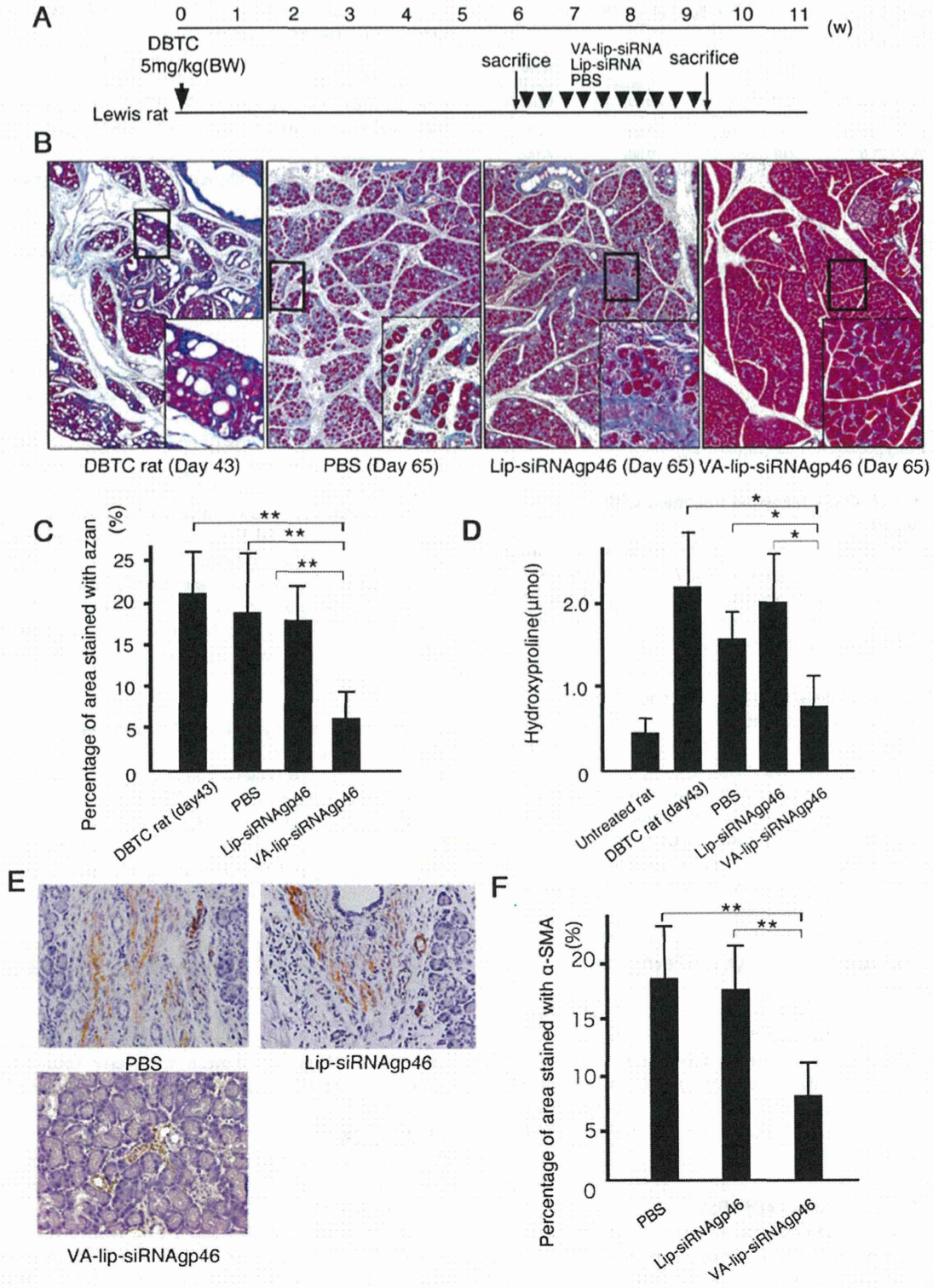

Figure 3 Effect of intravenous injected vitamin A-coupled liposomes (VA-lip-siRNAgp46) on dibutyltin dichloride (DBTC)-induced pancreatic fibrosis. (A) Schedule of VA-lip-siRNAgp46 treatment in rats with DBTC-induced pancreatic fibrosis. Samples were obtained from DBTC-treated rats that received 10 injections of VA-lip-siRNAgp46, Lip-siRNA gp46 (siRNA doses of 0.75 mg/kg, 3 times every other day), or PBS alone (n=10 per group). (B) Representative photomicrographs of Azan-Mallory stained pancreas section. Pictures were taken at original magnification (×100). Magnified images corresponding to the areas enclosed in boxes are presented as indicated. (C) Azan-Mallory positive staining area assessed by computerised image analysis. Data were obtained from six randomly selected fields in each of 10 rats from four groups and represent the mean±SD. (D) Hydroxyproline content in the pancreas. Mean±SD of 10 rats per group. (E) Representative immunohistochemical staining images of activated pancreatic stellate cells stained with anti-α-SMA antibody (brown). Pictures were taken at original magnification (×200). Results from each group of 10 rats were essentially similar. (F) α-SMA-positive staining area assessed by computerised image analysis. Data were obtained from six randomly selected fields in each of 10 rats from three groups and represent the mean±SD. *p<0.05; **p<0.01 vs VA-lip-siRNAgp46 treated- DBTC rat.

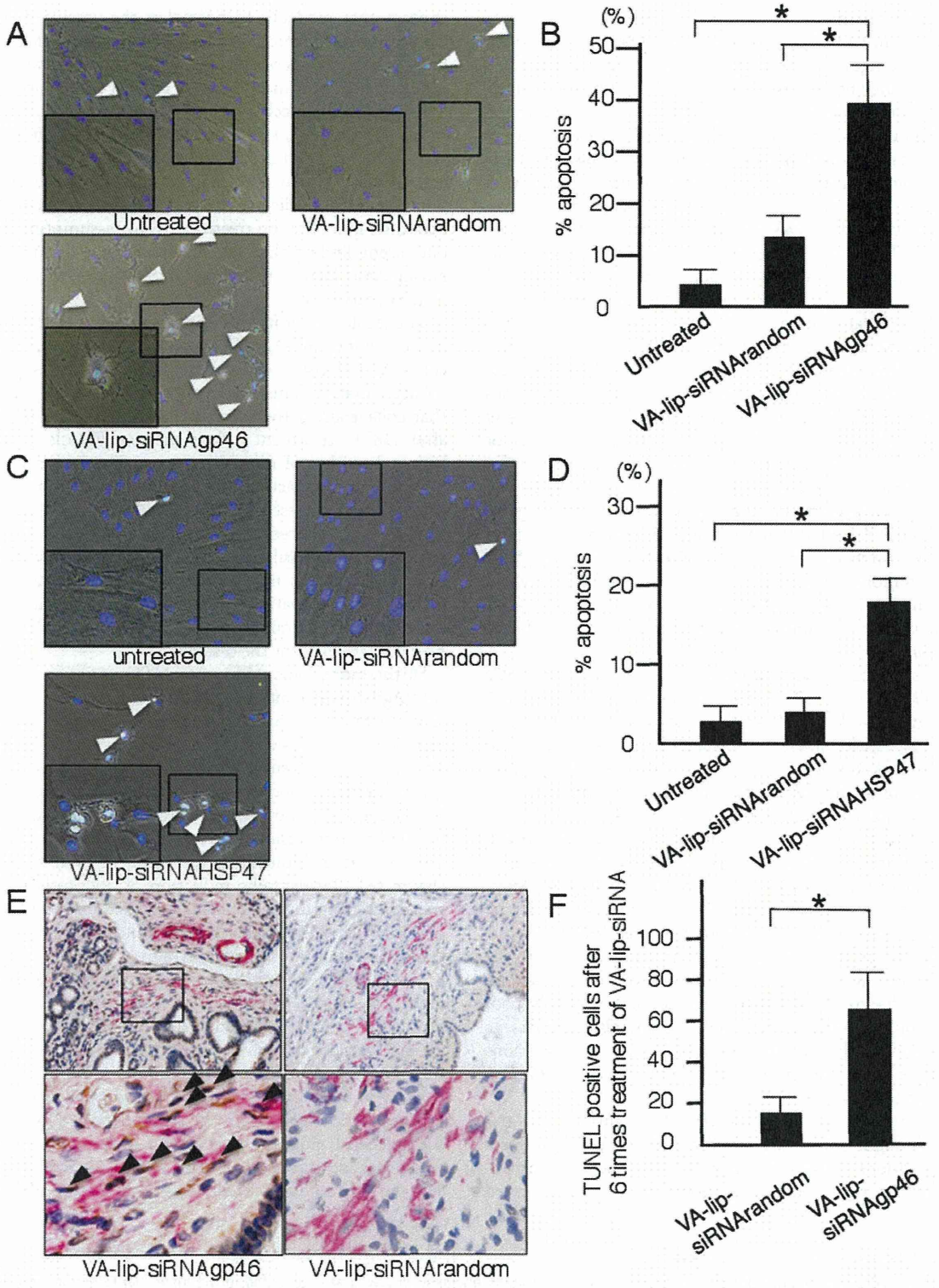

Figure 4 Apoptosis of activated pancreatic stellate cells (aPSCs) induced by vitamin A-coupled liposomes (VA-lip-siRNA) treatment. (A) Representative photomicrographs of rat aPSCs undergoing apoptosis. Nuclei of aPSCs treated with VA-lip-siRNAgp46 or with control agents were stained with FITC-transferase-mediated deoxyuridine triphosphate nick-end labelling (TUNEL) (green) and DAPI (blue) 72 h after each treatment. Arrowheads indicate apoptotic cells. Pictures taken at original magnification (×200) and magnified images corresponding to the areas enclosed in boxes are presented in the inset. (B) Quantification of apoptotic aPSCs shown in figure 4A. Apoptotic nuclei (green) and total nuclei (green + blue) were examined by fluorescent microscopy and counted in 10 randomly selected fields per slide for each indicated treatment; the ratios of apoptotic to normal nuclei were expressed as percentages. Results represent the mean±SD of three independent experiments. *$p<0.01$ vs VA-lip-siRNAgp46. (C) Representative photomicrographs of human aPSCs undergoing apoptosis. Nuclei of aPSCs treated with VA-lip-siRNAHSP47 or with control agents were stained with FITC-TUNEL (green) and DAPI (blue) 72 h after each treatment. Arrowheads indicate apoptotic cells. Pictures taken at original

Incidentally, regarding a possible role of other cellular components such as myofibroblasts in pancreatic fibrosis, it is rather difficult to distinguish it from that of aPSCs since when PSCs are activated, they become positive for α-SMA, which is characteristic of myofibroblasts. In this context, it should be noted that quiescent PSCs store vitamin A, and when they become myofibroblasts, although no more vitamin A droplets in their cytoplasm are observed, they still can take up vitamin A as shown by in vitro transfection experiments using VA-lip-siRNAgp46. This was true for hepatic stellate cells too. This is carefully discussed in our previous paper.[6] It is speculated that deposited vitamin A in quiescent cells may be used up or partly excreted on myofibrobrast transformation.

Prior to the examination of therapeutic effect, we assured specific delivery of VA-lip-siRNAgp46 to aPSCs in fibrotic pancreas tissue, demonstrating the mergence of the green fluorescence of siRNA-FAM encapsulated in vitamin A liposomes with the red fluorescence of α-SMA-positive cells (aPSCs), and higher accumulation of ^{3}H-VA-lipsiRNA in the pancreas of DBTC-treated rats than that in normal rats. The reason for 10-fold more radioactivity in the lung and intestine may be due to the higher content of macrophages in these organs. However, the 150-fold difference between liver and pancreas may not be simply ascribed to the difference in macrophage content, but more likely to the increased number of activated hepatic stellate cells since in this model, not only pancreas but also liver undergoes fibrosis because of obstruction of the common bile duct.

Collectively these results supported the notion that aPSCs preferentially take up siRNAgp46 encapsulated in vitamin A liposomes in vivo. We also examined the kinetics of the effect in vivo, prior to assessment of therapeutic efficacy, and found that the suppression of gp46 expression lasted for 3 days after the injection of VA-lip-siRNAgp46. Thus, our therapy protocol involved injecting the drug three times per week.

The therapeutic effect of treatment, namely, histological improvement and normalised hydroxyproline levels in the pancreas, was observed following administration of drug 10 times. In our previous study using liver cirrhosis models, substantial resolution of fibrotic tissue was obtained after only five treatments.[6] In the present study, we also initially used only five treatments, but improvement of fibrosis was unsatisfactory. This may be due to the fact that the pancreas is relatively poor in blood supply compared with the liver, and thus the dosage of siRNAgp46 at the fibrotic loci supplied by five injections may not have been sufficient to bring about effective resolution of pancreatic fibrosis.

Incidentally, it may be noteworthy to mention that our treatment brought about less vessel density since it promises wider implications such as depletion of tumour stroma in pancreas cancer. In this regard, it is nowadays a well accepted concept that modality to normalise the vascularity by diminishing immature microvessels with anti-neoangiogenesis antibody, rather enhances the efficacy of chemotherapy when the antibody and anticancer drug are used in combination.[22]

Regarding the mechanism for the enhanced microvascularity in fibrotic tissue and decrement of vascularity after treatment, we assume, in good agreement with reports by and Hideshima and Okada,[23 24] that aPSCs are producing angiogenesis factor(s) which will be eradicated from the tissue in accordance with apoptosis induction by treatment. This assumption is based on our recent finding that rat aPSCs are indeed expressing some angiogenesis factors, including fibroblast growth factor (unpublished observation).

The resolution of fibrosis appears to occur by a dual mechanism involving siRNAgp46, which inhibits de novo secretion of collagen, and tissue collagenase, which dissolves predeposited collagen matrix. This assumption is consistent with the fact that collagenase activity in the pancreas at day 42 and day 49 after DBTC treatment, when massive fibrosis occurred, was higher than that of normal pancreas. The reason for sustained high collagenase activity after VA-lip-siRNAgp46 treatment, despite the suppressed MMP2 mRNA, may be that TIMP from aPSCs is also reduced due to apoptosis of aPSCs. In addition, a persistent extracellular matrix pool of collagenase after it is secreted from cells may account for the sustained collagenase activity.[25 26] Activation of matrix metalloproteinases (MMPs) derived from inflammatory cells by reduced TIMP-1 expression may also account for the discrepancy.

Furthermore, apoptosis of aPSCs via transduction of siRNAgp46 was confirmed in our vitro experiment, indicating that a similar mechanism is involved in apoptosis of aHSCs and aPSCs. It is plausible that collagen secreted by aHSCs and aPSCs serves as a survival signal and that this signal is abrogated, leading to apoptosis, as a result of collagen degradation by collagenase (unpublished observation). In support of this possibility, our results demonstrated that high collagenase activity was maintained in the pancreas even after treatment (figure 6C). Incidentally, induction of apoptosis by inhibiting collagen secretion was confirmed to occur even in human PSCs treated with VA-lip-siRNAHSP47, indicating applicability of this approach in the clinical setting.

Interestingly, inflammation associated with fibrosis in this model was also decreased by this treatment, probably due to the fact that aPSCs, which were eradicated by our treatment, are involved not only in the development of fibrosis but also in the inflammatory reaction.[21]

Liver fibrosis in DBTC-treated rats was also successfully resolved with treatment in the present study. However, because the epithelial plug in the common duct was not removed by the treatment, increased serum amylase, alanine aminotransferase and bilirubin persisted (data not shown). In the DBTC

magnification (×200) and magnified images corresponding to the areas enclosed in boxes are presented in the inset. (D) Quantification of apoptotic aPSCs shown in figure 4C. Apoptotic nuclei (green) and total nuclei (green + blue) were examined by fluorescent microscopy and counted in 10 randomly selected fields per slide for each indicated treatment; the ratios of apoptotic to normal nuclei were expressed as percentages. Results represent the mean±SD of three independent experiments. *$p<0.01$ vs VA-lip-siRNAHSP47. (E) Representative immunohistochemical staining of pancreas specimens from dibutyltin dichloride (DBTC) (5 mg/kg) treated rats (day 56) that received six injections of VA-lip-siRNAgp46 (left panel) or VA-lip-siRNArandom (right panel) (siRNA doses of 0.75 mg/kg, 3 times every other day) stained for TUNEL (brown, arrowhead) and α-SMA (red). Magnified images of the corresponding areas in boxes indicated that the number of cells with TUNEL-positive overlapping of α-SMA-positive PSCs was substantially increased in VA-lip-siRNAgp46 specimens compared with VA-lip-siRNArandom specimens. Pictures were taken at original magnification (×100). (F) Quantification of TUNEL-positive PSCs in pancreas specimens from VA-lip-siRNAgp46-treated DBTC-rats and VA-lip-siRNArandom. The number of TUNEL-positive cells in α-SMA-positive areas was counted in 10 randomly selected fields per pancreas section of each rat. *$p<0.01$. The results were essentially similar within each group of three rats.

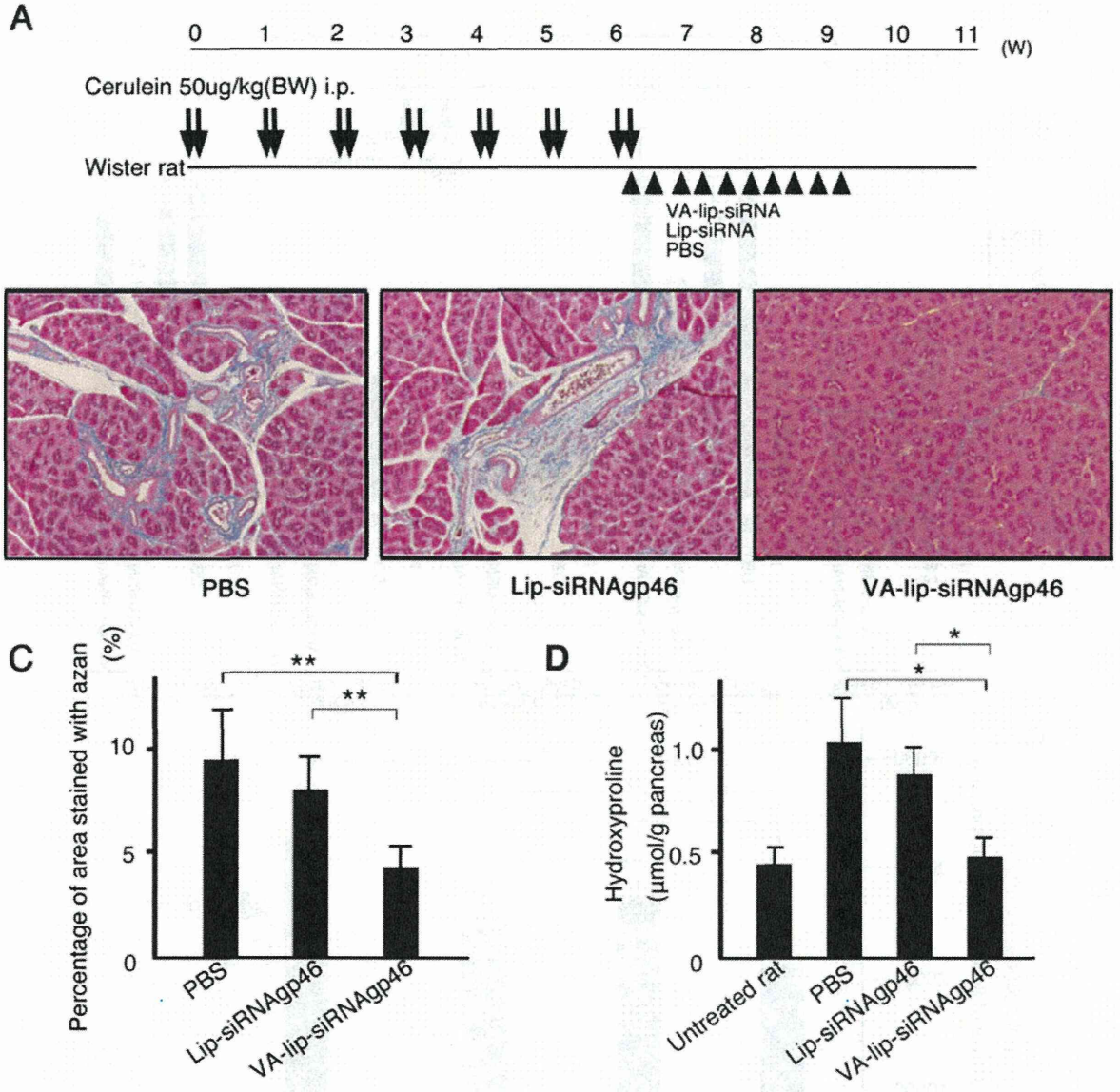

Figure 5 Effect of intravenous injected vitamin A-coupled liposomes (VA-lip-siRNAgp46) on cerulein-induced pancreatic fibrosis. (A) Schedule of VA-lip-siRNAgp46 treatment in rats with cerulean-induced pancreatic fibrosis. Samples were obtained from cerulean-treated rats that received 10 injections of VA-lip-siRNAgp46, Lip-siRNA gp46 (siRNA doses of 0.75 mg/kg, 3 times every other day) or PBS alone (n=10 per group). (B) Representative photomicrographs of an Azan-Mallory-stained pancreas section. Pictures taken at original magnification (×100). (C) Azan-Mallory-positive staining area assessed by computerised image analysis. Data were obtained from six randomly selected fields in each of 10 rats from three groups and represent the mean±SD. (D) Hydroxyproline content in the pancreas. Mean±SD of 10 rats per group. *p<0.05; **p<0.01 vs VA-lip-siRNAgp46 treated-dibutyltin dichloride rat.

model, unlike in advanced chronic pancreatitis in humans, β-cells remained intact and, therefore, no change in blood glucose levels was observed throughout the experimental period (data not shown).

To further evaluate the therapeutic effect of our modality in another model, we established a chronic pancreatitis model based on repeated administration of cerulein to rats.[12 18] The results in this model were compatible with those of the DBTC model, confirming the general efficacy of our modality in dissimilar pancreatic fibrosis models.

Off-target effects and stimulation of toll-like receptors (TLRs) are both critical issues to be solved in the application of therapies using siRNA. Since we used the same siRNA as that of the previous study on liver cirrhosis in which we denied a bystander effect by demonstrating comparable gene silencing efficacy and antifibrotic effect with two other independent siRNAs against the same target,[6] we believe it is unlikely to be the case.

Nonetheless, for future clinical applications, it will be necessary to conduct careful explorations of adverse effects, off-target effects and TLR stimulation.

In conclusion, the present data clearly indicate the therapeutic potential of our modality for pancreas fibrosis and suggest its potential for the treatment of organ fibrosis.

Contributors HI, YS and KM designed research, performed experiments and wrote the paper. AY, RF, HN, NB, TH, TS, KM, RT, MK, SA, YK, KH and JK performed experiments. YN designed research, wrote the paper and supervised the whole project. All authors discussed the results and commented on the manuscript.

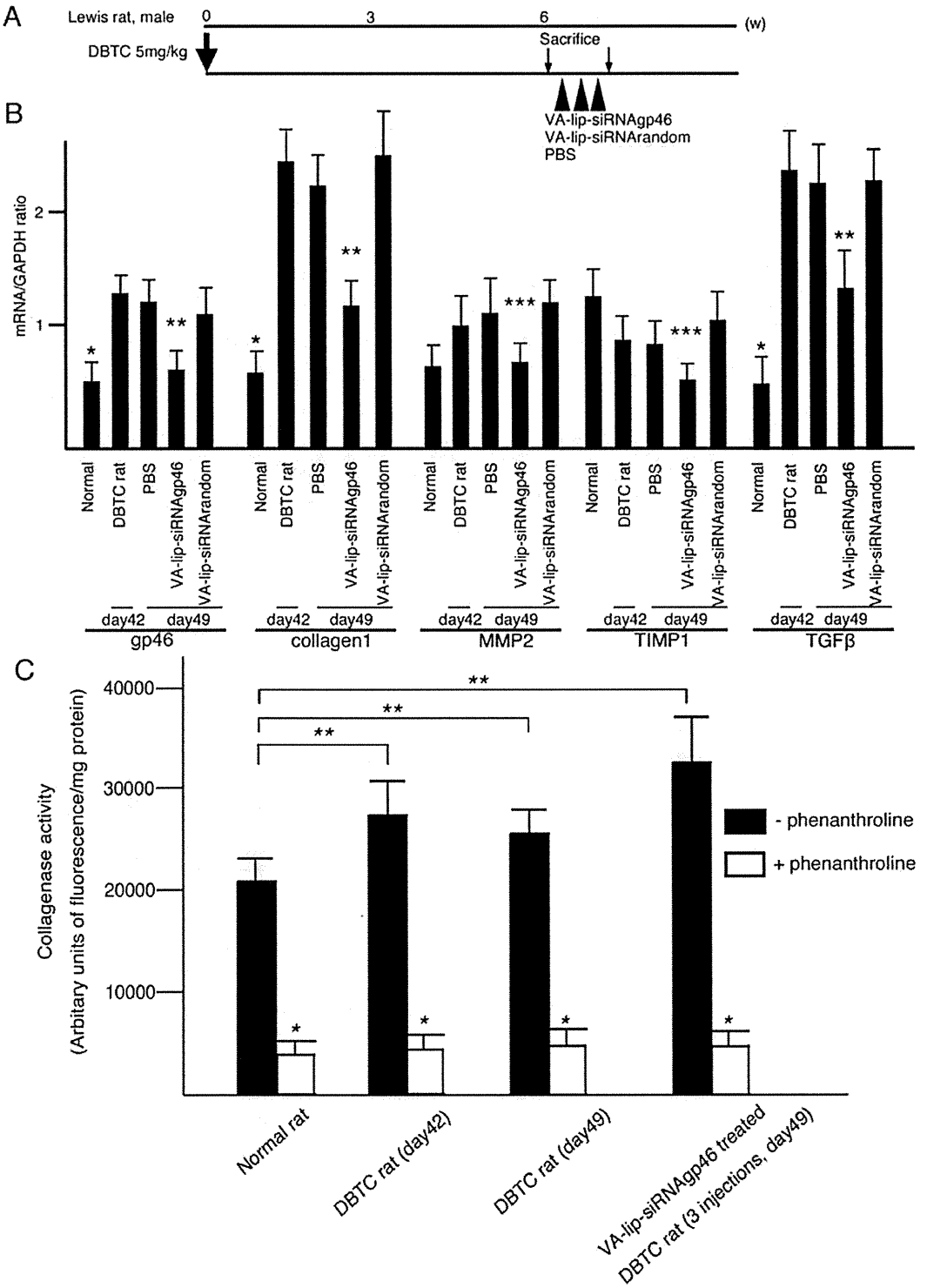

Figure 6 Effect of vitamin A-coupled liposomes (VA-lip-siRNAgp46) treatments on mRNA expression of fibrosis-related proteins and collagenase activity in pancreas homogenates. (A) Schedule of VA-lip-siRNAgp46 treatment in rats with dibutyltin dichloride (DBTC)-induced pancreatic fibrosis. Samples were obtained from DBTC-treated rats that received three injections of VA-lip-siRNAgp46, Lip-siRNA gp46 (siRNA doses of 0.75 mg/kg, 3 times every other day), or PBS alone (n=3 per group). (B) The expression of gp46, procollagen I, MMP-2, TIMP-1, and TGFβ mRNA in normal rats, DBTC-treated rats treated with three injections of PBS, DBTC-treated rats treated with three injections of VA-lip-siRNArandom, and DBTC-treated rats treated with three injections of VA-lip-siRNAgp46 were quantitated by real-time PCR. Expression was normalised as the ratio to GAPDH mRNA, a housekeeping gene. *$p<0.01$ vs DBTC rat (day42). **$p<0.01$ vs PBS (day46). ***$p<0.05$ vs PBS (day46). (C) Total collagenase activity in pancreas homogenates from normal rats, DBTC-treated rats (day 42), DBTC-treated rats (day 49), and DBTC rats treated with three injections of VA-lip-siRNAgp46 (siRNA doses of 0.75 mg/kg, 3 times every other day, day 49) in the absence or presence of MMP inhibitor (1,10-phenanthroline). Results are the mean±SD of five rats per group. *$p<0.01$ vs without inhibitor. **$p<0.05$ vs normal rat.